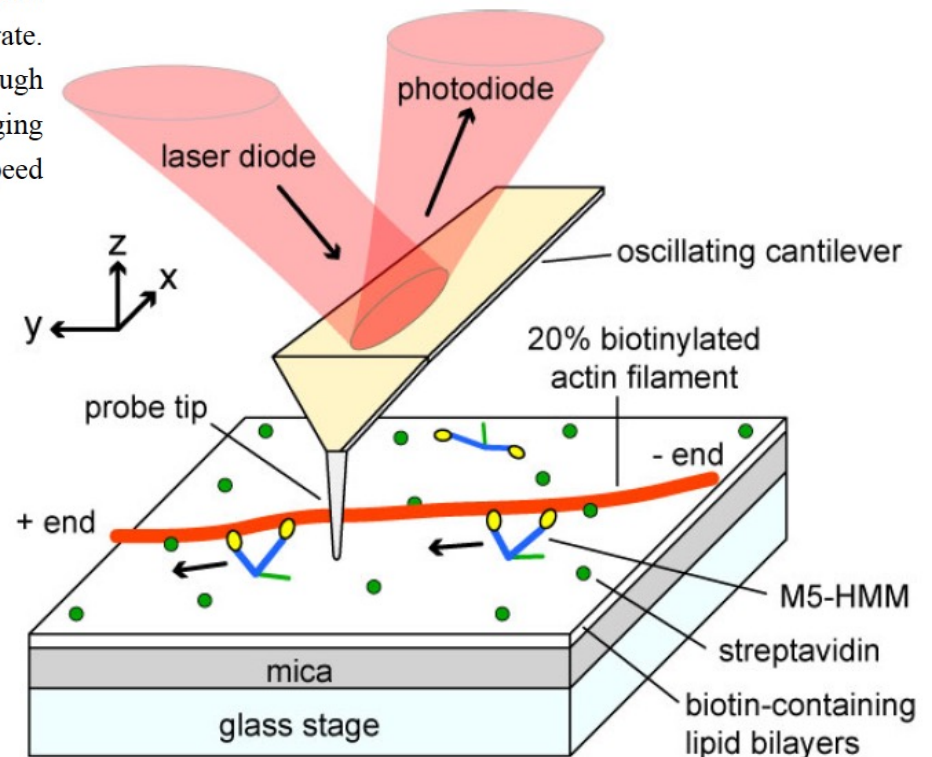# ATOMIC FORCE MICROSCOPY
Imaging in Biology_2
Examples

Myosine V walking on actin filaments

Video imaging by high-speed AFM has been applied to capture the dynamic behaviour of myosin V (two headed motor that functions as cargo transporter in cells) translocating along an acting filament. Moves hand-over-hand, 36 nm per ATP hydrolysis

Supplementary Figure 1 | Schematic of assay system for HS-AFM imaging (not scaled). A mica surface was fully covered with biotin-containing lipid bilayers. Streptavidin molecules (green circles) were partially deposited on the substrate. Biotinylated actin filaments were immobilised on the bilayer surface through streptavidin molecules. M5-HMM was deposited on the lipid bilayers. All imaging experiments were performed in the tapping mode using a laboratory-built high-speed AFM apparatus[5,6].

A positively charged lipid in the mixed lipid bilayer was necessary to assure weak interaction with Myosine and translocation along the actin filament

N. Kodera, D. Yamamoto, R. Ishikawa, T. Ando *Nature* **468**, 72 (2010)

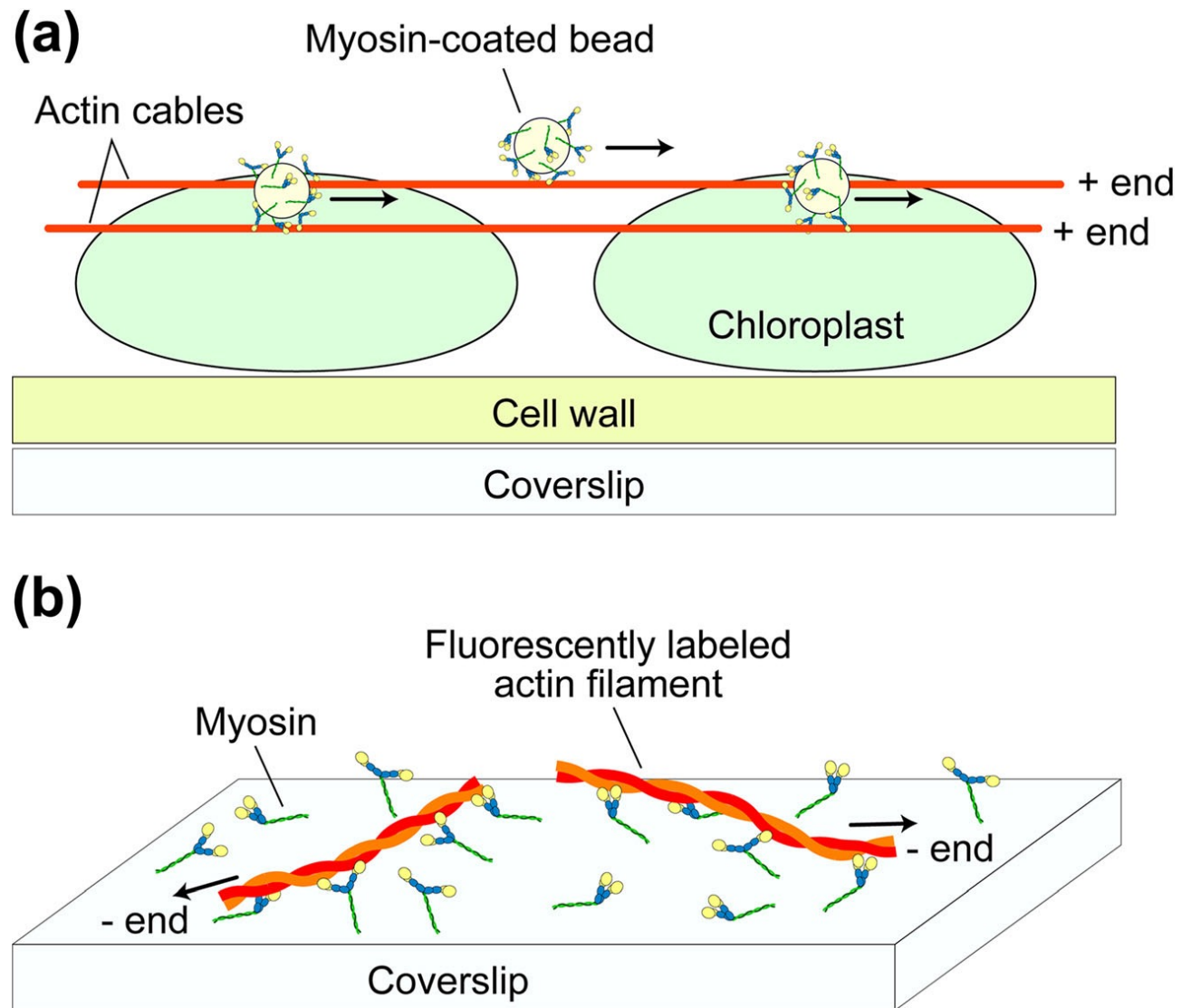# Myosine V walking on actin filaments

Each head of the double-headed myosin hydrolyzes ATP into ADP and inorganic phosphate (Pi). The ATPase rate is very low when myosin is alone but is markedly accelerated by its interaction with actin, where the chemical energy liberated by ATP hydrolysis is converted into mechanical work.
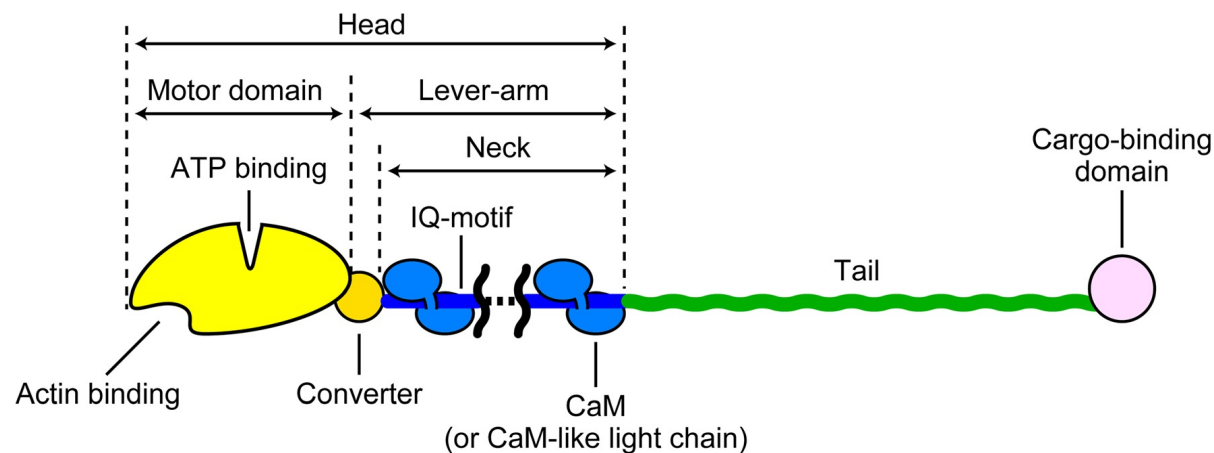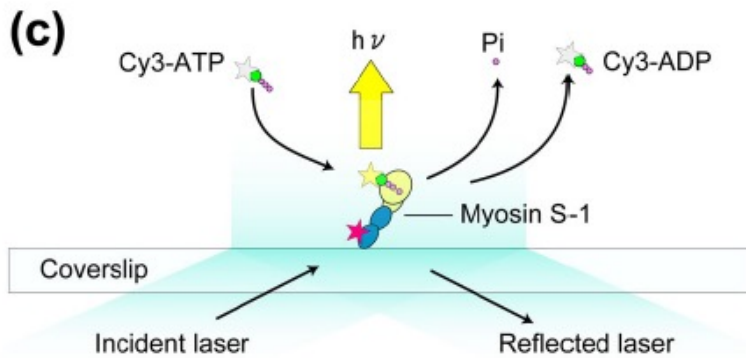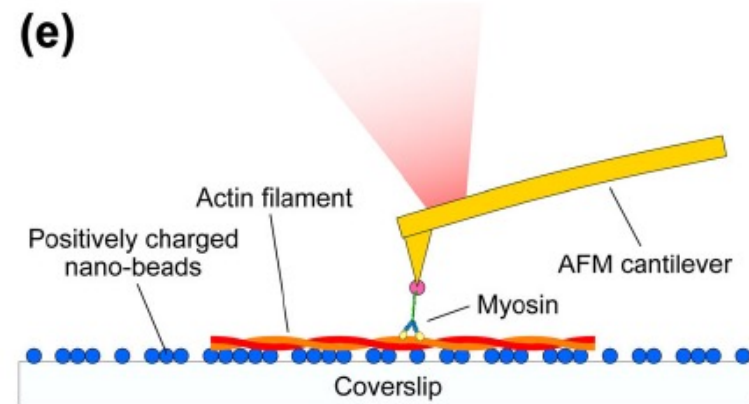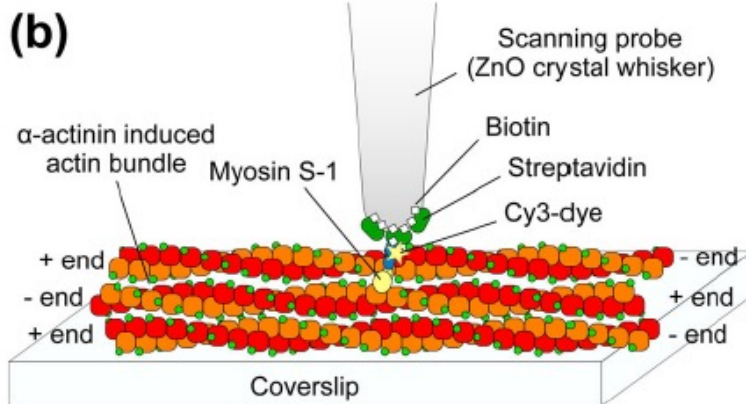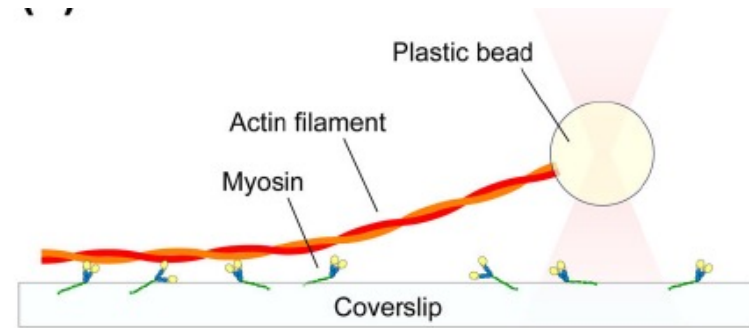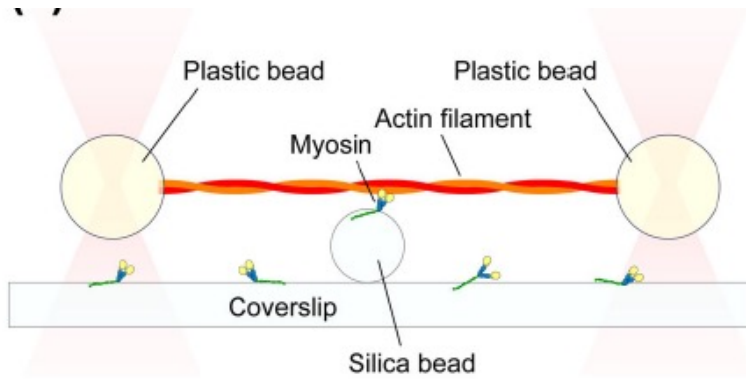

High-speed atomic force microscopy (HS-AFM), allow video-recording the structure and dynamics of functioning biomolecules at single-nanometer resolution, without disturbing their function. It helped to discover that the tension responsible for forward movement can be generated without any chemical transition, meaning that no chemical energy input is required for the tension generation.

Moreover, the lever-arm swing (powerstroke) by the leading head spontaneously occurs when the trailing head detaches, thus demonstrating that no chemical energy input is required for the lever-arm swing either.

Fig. 4 Schematics showing in vitro motility assay systems for actomyosin. **a** Myosin-coated bead assay. The myosin-coated fluorescent beads are subjected to the polar arrays of actin cables naturally formed on chloroplastd of the alga *Nitella*, and movement of the beads are observed under a florescent microscope. **b** Actin filament gliding assay. Myosin molecules are attached to the surface of a nitrocellulose-coated coverslip and gliding motion of the fluorescently labeled actin filaments are observed under a fluorescence microscope
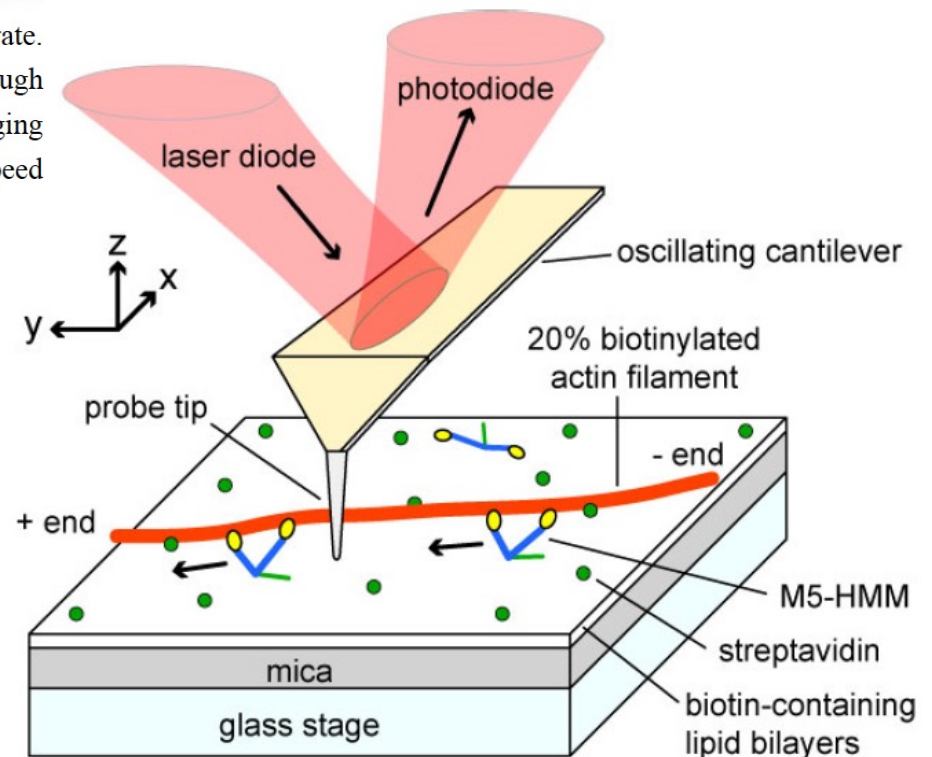
(a)

Myosin-coated bead

Actin cables

+ end
+ end

Chloroplast

Cell wall

Coverslip

(b)

Fluorescently labeled actin filament

Myosin

- end

- end

Coverslip

(b)

(c)

(e)

Plastic bead

Plastic bead

Actin filament

Myosin

Coverslip

Silica bead

Plastic bead

Actin filament

Myosin

Coverslip

Scanning probe
(ZnO crystal whisker)

α-actinin induced
actin bundle

Myosin S-1

Biotin

Streptavidin

Cy3-dye

+ end

− end

− end

+ end

+ end

− end

Coverslip

Actin filament

Positively charged
nano-beads

Myosin

AFM cantilever

Coverslip

Cy3-ATP

hν

Pi

Cy3-ADP

Myosin S-1

Coverslip

Incident laser

Reflected laser

5

Myosine V walking on actin filaments

Also, video imaging by high-speed AFM has been applied to capture the dynamic behaviour of myosin V (two headed motor that functions as cargo transporter in cells) translocating along an acting filament. Moves hand-over-hand, 36 nm per ATP hydrolysis

Supplementary Figure 1 | Schematic of assay system for HS-AFM imaging (not scaled). A mica surface was fully covered with biotin-containing lipid bilayers. Streptavidin molecules (green circles) were partially deposited on the substrate. Biotinylated actin filaments were immobilised on the bilayer surface through streptavidin molecules. M5-HMM was deposited on the lipid bilayers. All imaging experiments were performed in the tapping mode using a laboratory-built high-speed AFM apparatus[5,6].

A positively charged lipid in the mixed lipid bilayer was necessary to assure weak interaction with Myosine and translocation along the actin filament

N. Kodera, D. Yamamoto, R. Ishikawa, T. Ando *Nature* **468**, 72 (2010)

Myosine V walking on actin filaments

AFM images demonstrate a hand-over-hand movement, with swinging lever-arm motion : the detached T-head rotationally diffused around the advancing neck-neck junction. Extra STV needed as an "obstacle" to slow down the motion to be visualized (100 ms/frame)
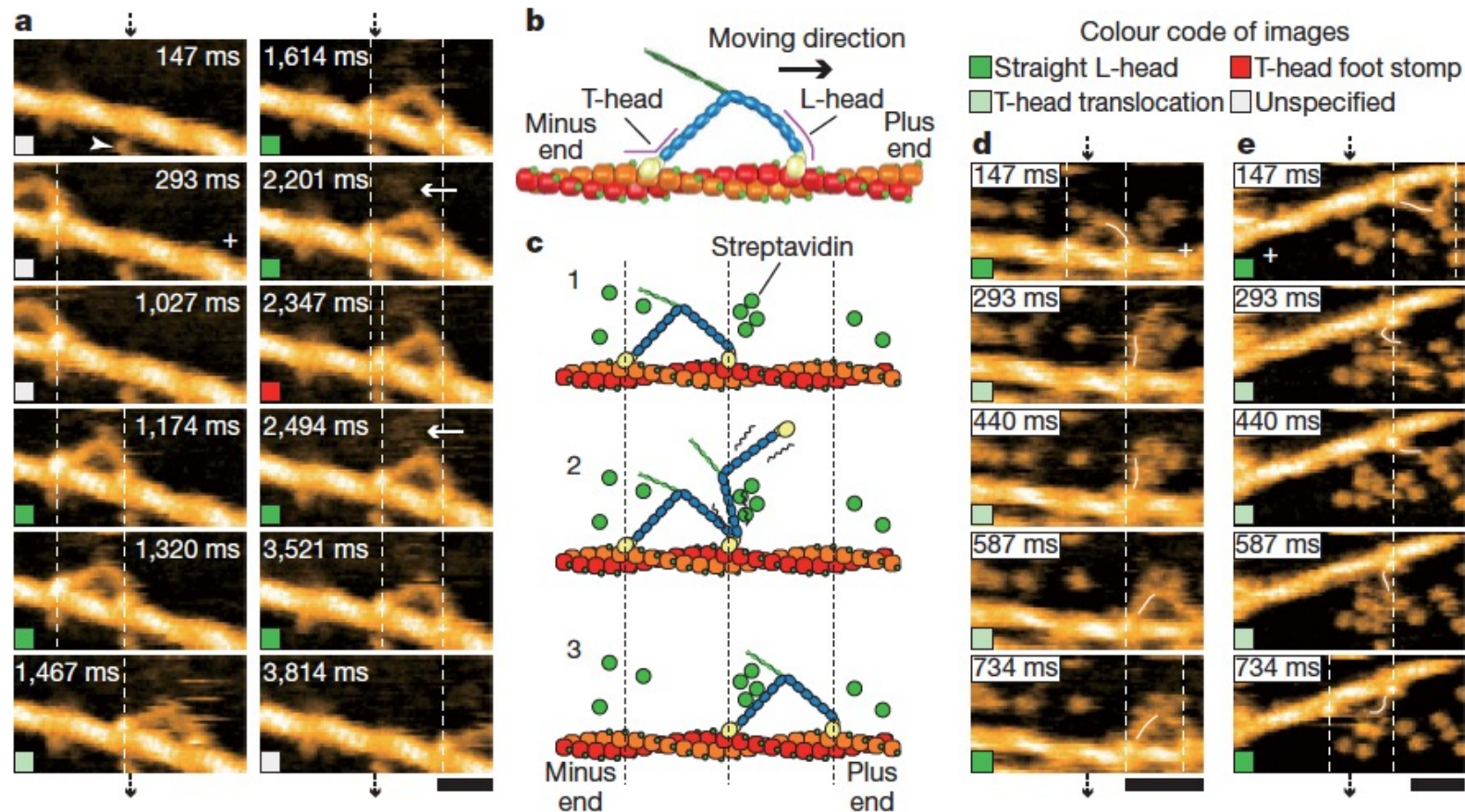
N. Kodera, D. Yamamoto, R. Ishikawa, T. Ando *Nature* **468**, 72 (2010)

http://biophys.w3.kanazawa-u.ac.jp/M5_movies.htm

Myosine V walking on actin filaments

The neck–motor domain junction appears smooth in the leading head (L-head) but is V-shaped in the trailing head (T-head) without exception.
The short coiled coil tail was mostly tilted towards the minus end of actin

N. Kodera, D. Yamamoto, R. Ishikawa, T. Ando *Nature* **468**, 72 (2010)

http://biophys.w3.kanazawa-u.ac.jp/M5_movies.htm

Myosine V walking on actin filaments

The neck–motor domain junction appears smooth in the leading head (L-head) but is V-shaped in the trailing head (T-head) without exception.
The short coiled coil tail was mostly tilted towards the minus end of actin

N. Kodera, D. Yamamoto, R. Ishikawa, T. Ando *Nature* **468**, 72 (2010)

http://biophys.w3.kanazawa-u.ac.jp/M5_movies.htm
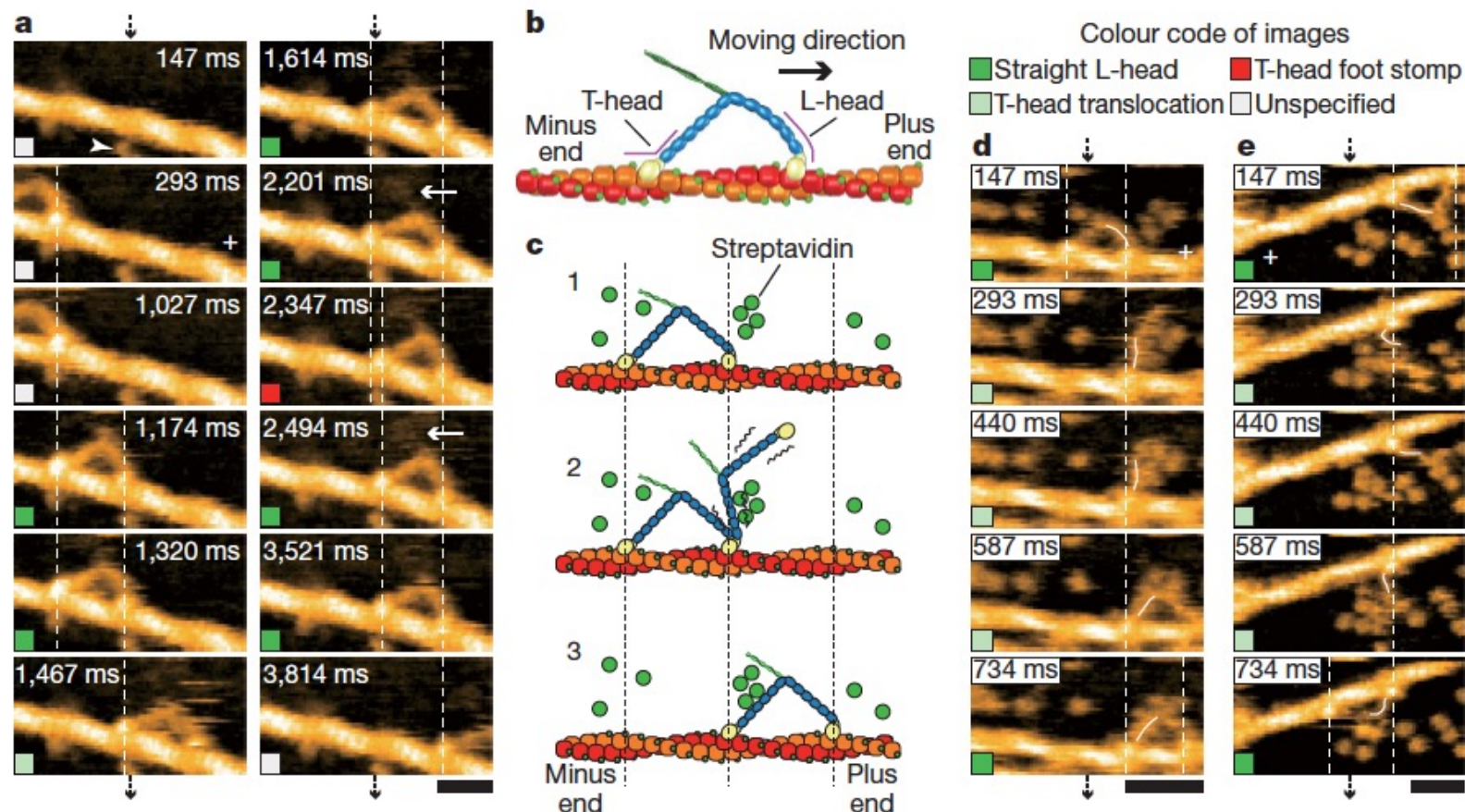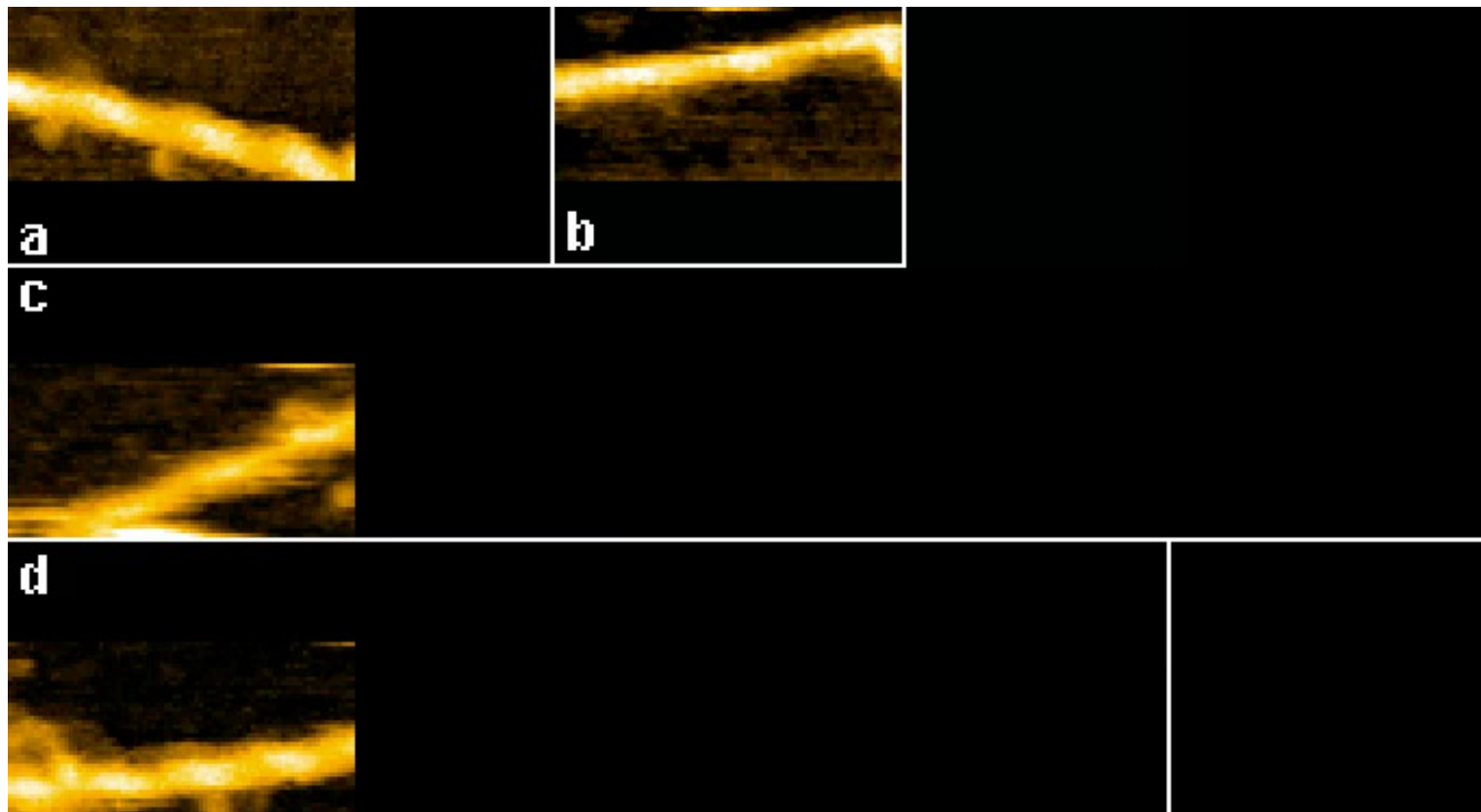
Myosine V walking on actin filaments

After T-head detachment, the nearly straight leading neck swung from the reverse arrowhead (R-ARH) orientation to the arrowhead (ARH) orientation (Supplementary Movie 2), confirming the swinging lever-arm motion initially proposed for muscle myosin. The detached T-head rotationally diffused around the advancing neck–neck junction (no translational diffusion on the actin occurs) and then bound to a forward site on the actin filament, completing one step.
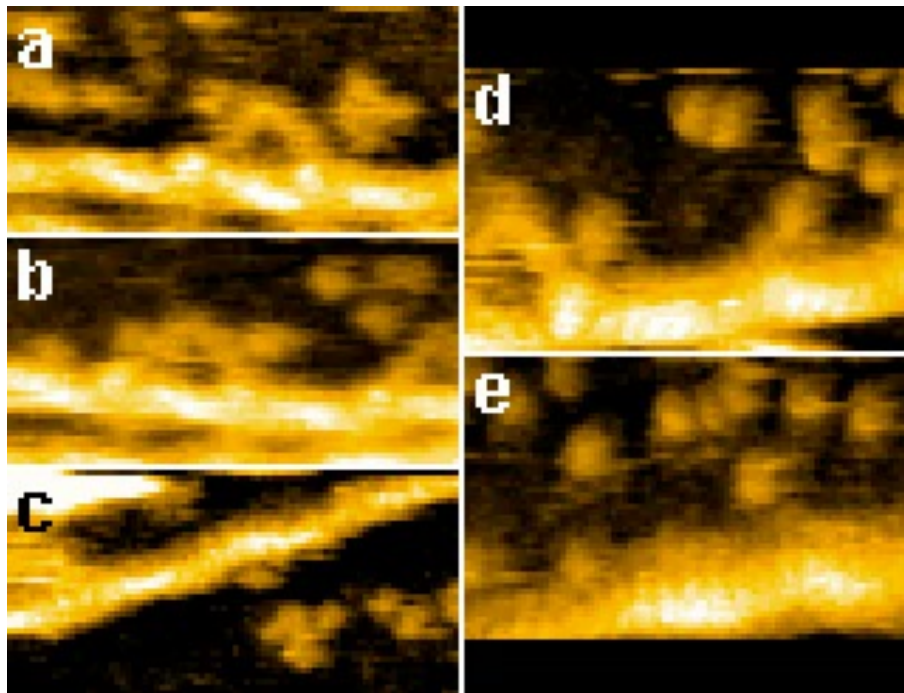
The captured images show that the forward movement is driven not by bending but by rotation of the L-head. The rotation seems to occur spontaneously after T-head detachment, suggesting that intramolecular tension driving the L-head swing exists in the two-headed bound molecules.

N. Kodera, D. Yamamoto, R. Ishikawa, T. Ando *Nature* **468**, 72 (2010)

Myosine V walking on actin filaments
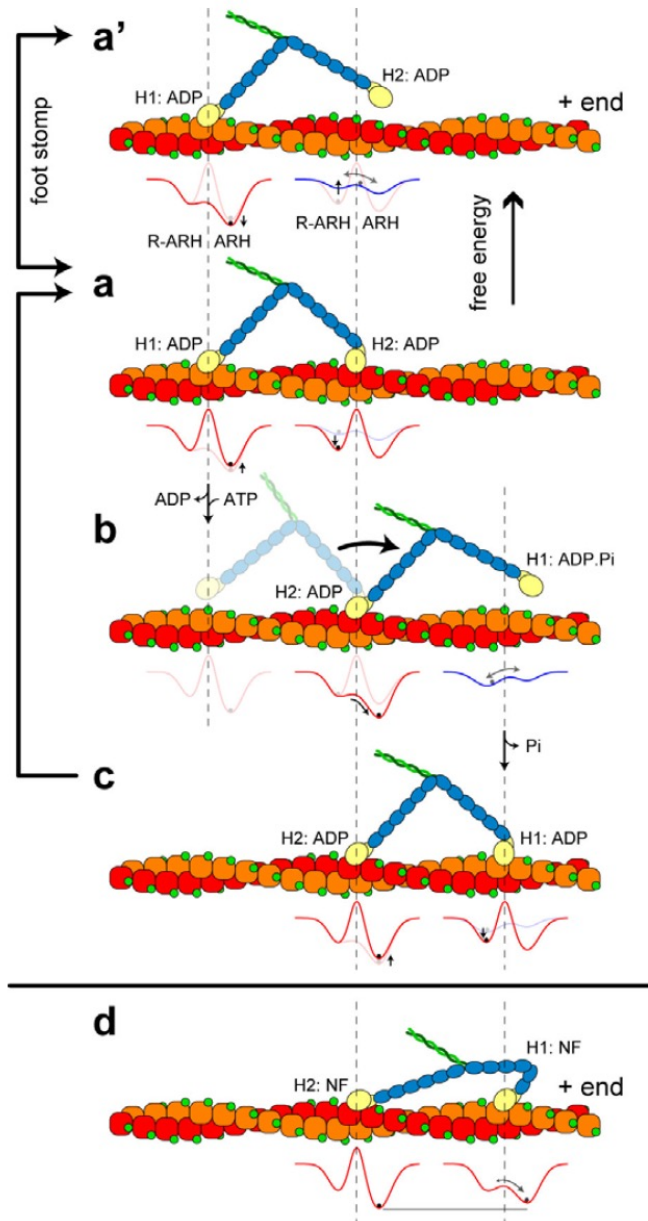
In dynamic HS-AFM the molecule itself is visualized while working and moving on its biological track, providing concomitant structural and dynamic data: not only did the observation confirm the hand-over-hand walking mechanism of myosin-V, it did reveal that the power stroke of this motor is driven by intramolecular mechanical tension

N. Kodera, D. Yamamoto, R. Ishikawa, T. Ando *Nature* **468**, 72 (2010)

Single molecule imaging

HR-AFM imaging: DNA

Also, high-resolution AFM imaging has been recently employed to study topological details of DNA/RNA – enzymes interaction. For example, the upstream interaction of Escherichia coli RNA polymerase (RNAP) in an open promoter complex (RPo) formed at the PR and PRM promoters of bacteriophage λ.

I. Mangiarotti, S. Cellai, W. Ross, C. Bustamante, C. Rivetti, *L. Mol. Biol.* **385**, 748 (2009)
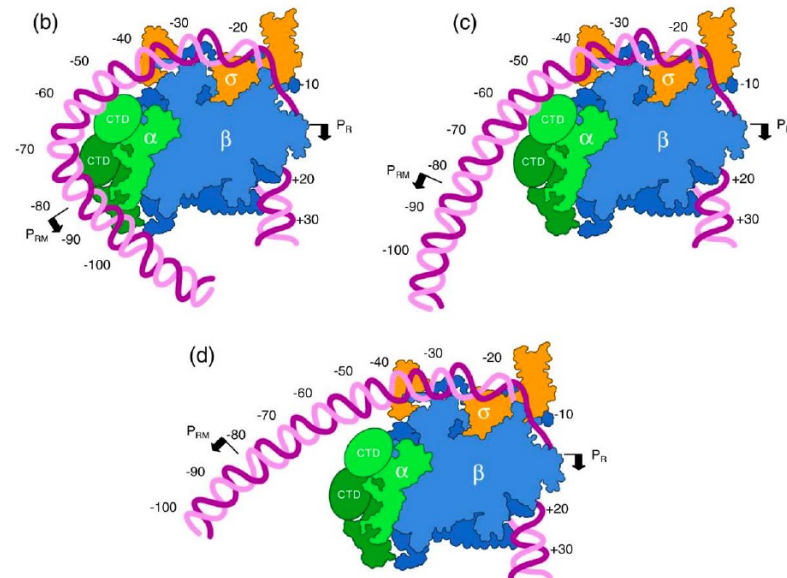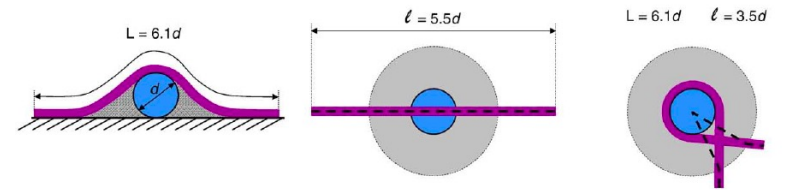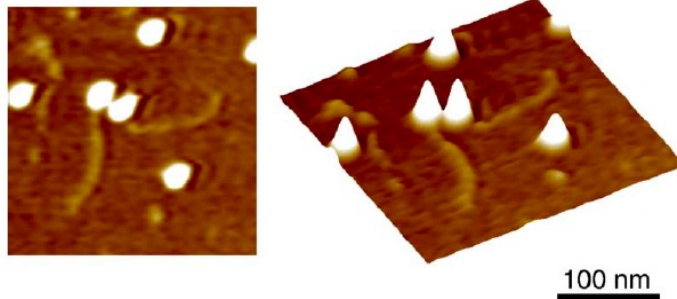
Prokaryotic transcription

Core promoter   Position +1

DNA

RNA polymerase attaches to the core promoter

RNA polymerase

Conversion of closed to open promoter complex

Initiation of RNA synthesis

Promoter clearance

RNA
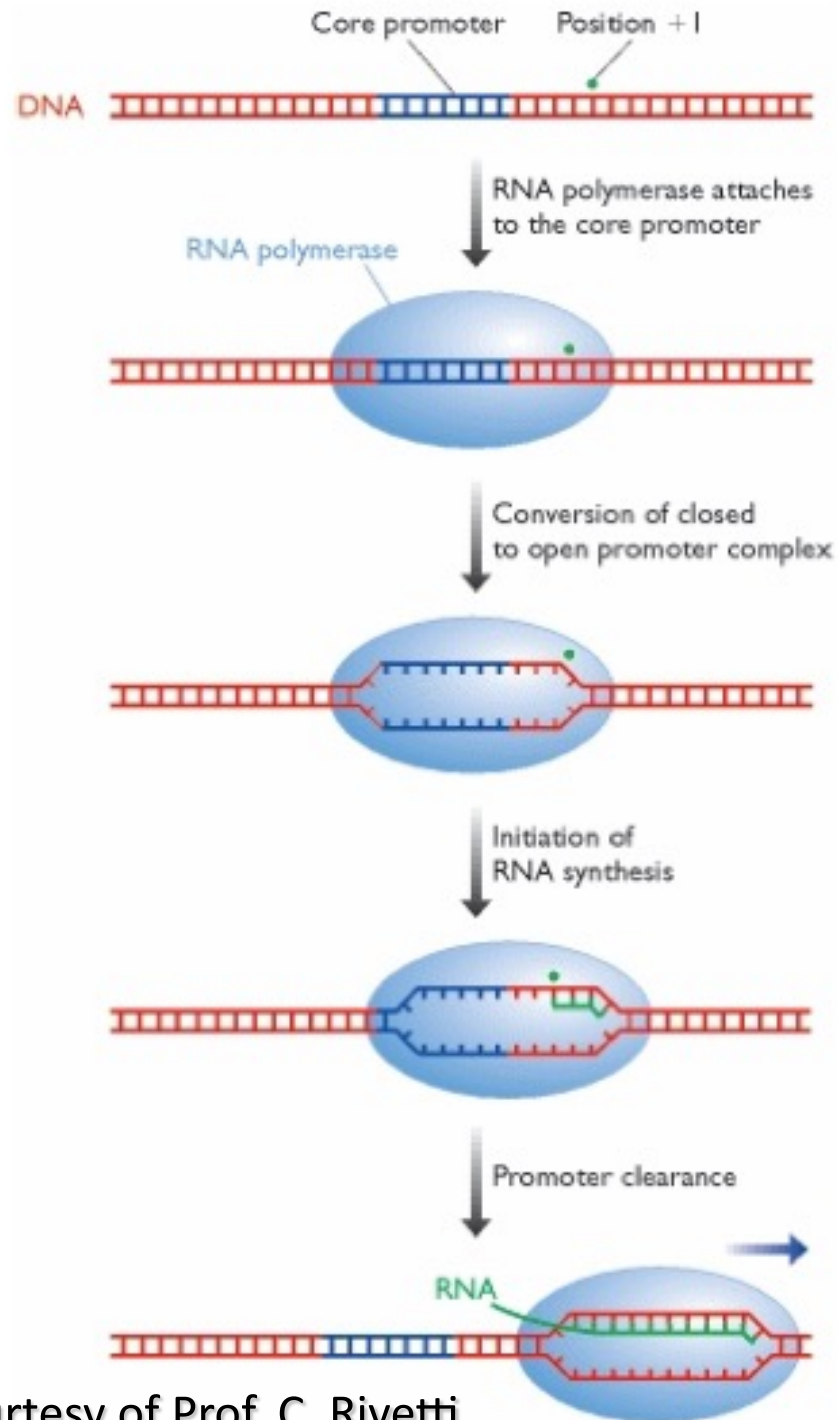
Courtesy of Prof. C. Rivetti

Struttura del DNA

coda 5'

Adenina

Timina

coda 3'

Scheletro
fosfato-
deossiribosio

coda 3'

Guanina

Citosina

coda 5'

∅ = 2 nm

3.4 nm
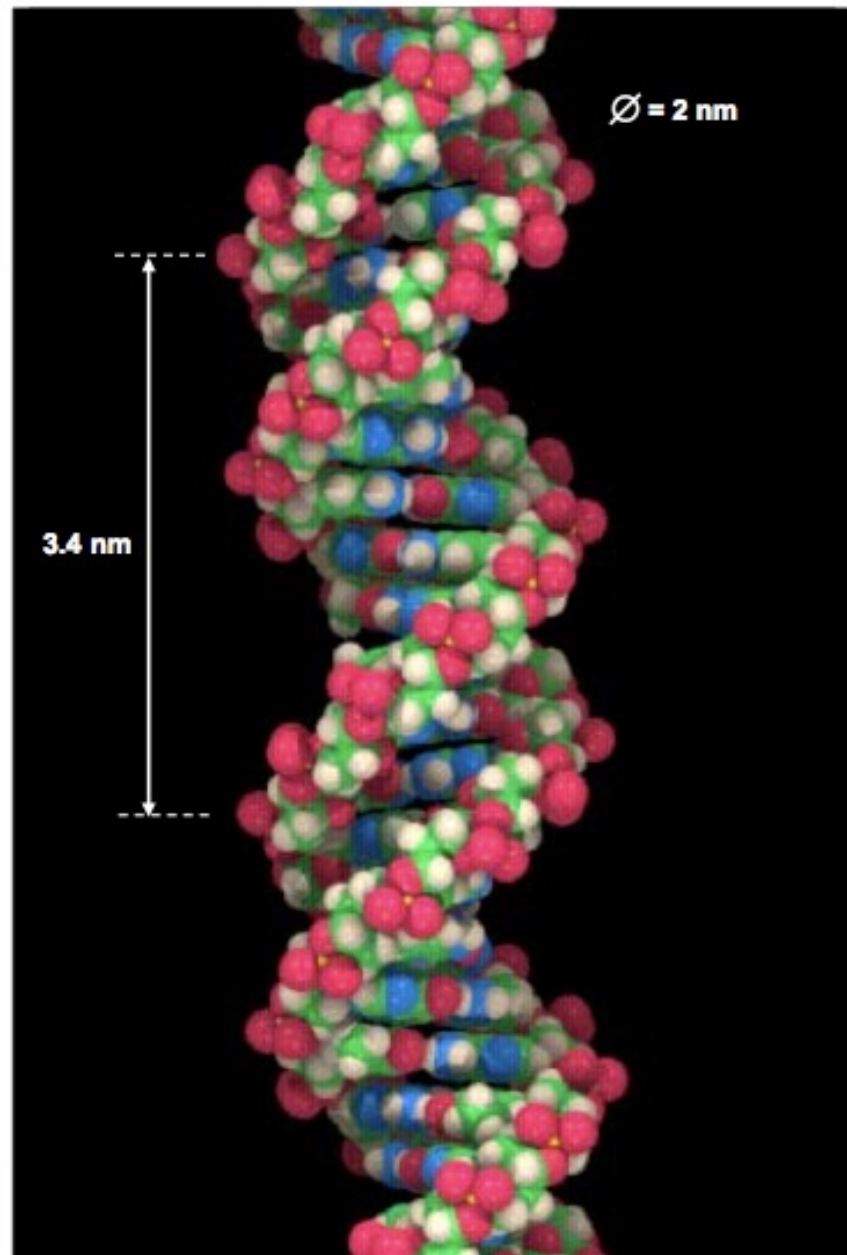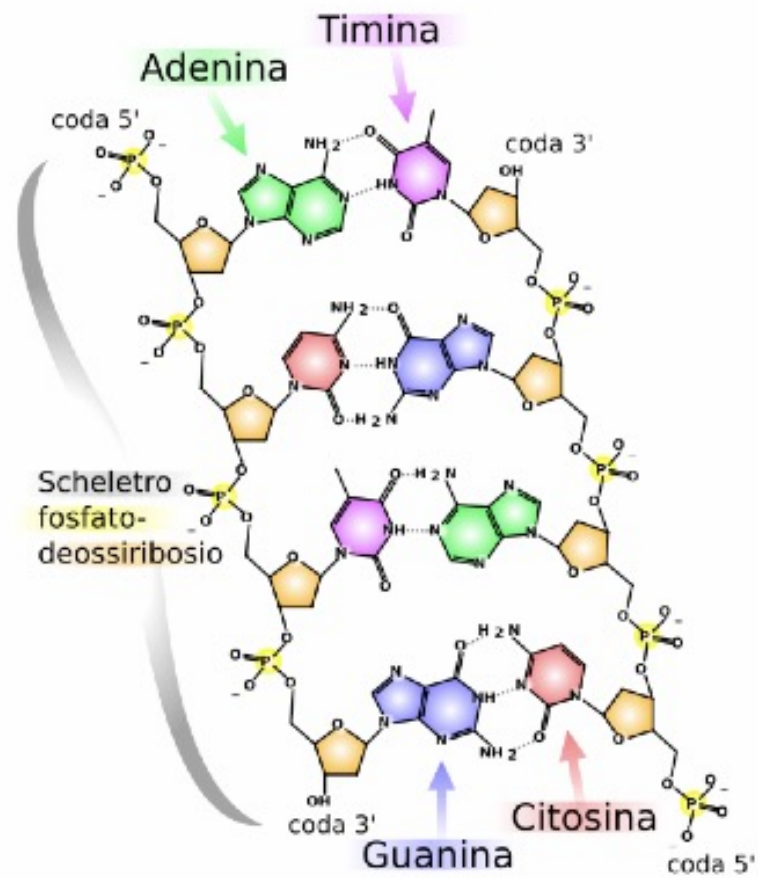
DNA

Watson and Crick, 1953
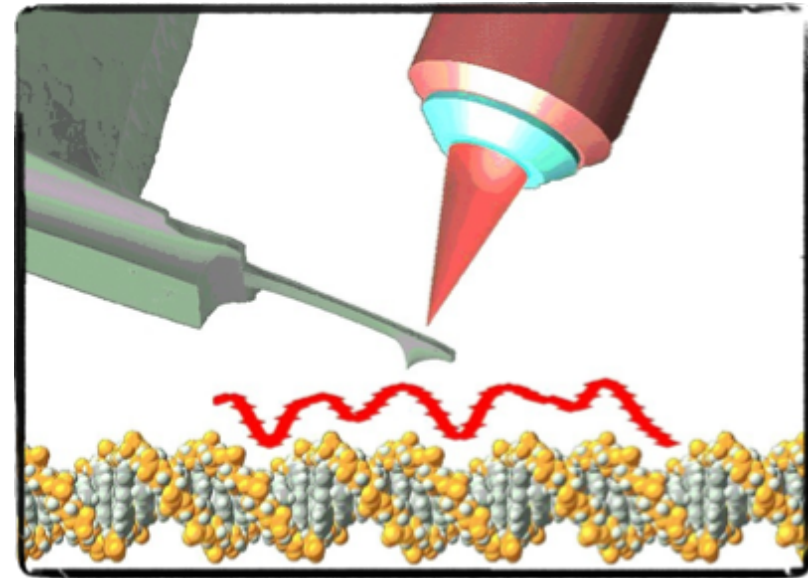
Leung et al., Nanoletters 2012

5' 3'

0.34 nm

Minor groove

3.4 nm

Major groove

3' 5'

(a) Miniaturized cantilever

20 µm

Conventional cantilever

(b) 10 µm

(c)

Amplitude [nm]   Thermal Noise [fm/√Hz]

0.8   30

0.5   20

0.2   10

1.00 1.25 1.50 1.75 2.00
Frequency [MHz]
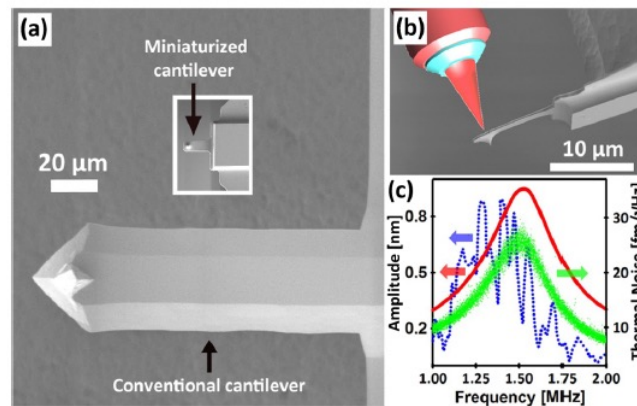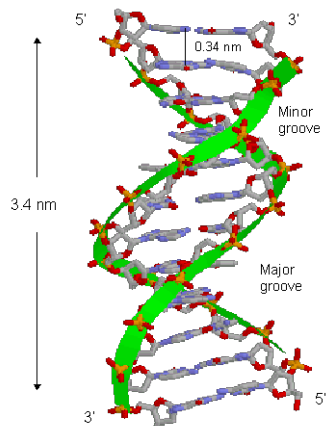
AFM image simulation of DNA

Rc = 7.0 nm   Rc = 5.0 nm   Rc = 4.0 nm   Rc = 2.0 nm

Rc = 1.0 nm   Rc = 0.5 nm   Rc = 0.1 nm

20 nm

Rc = 0.1 nm
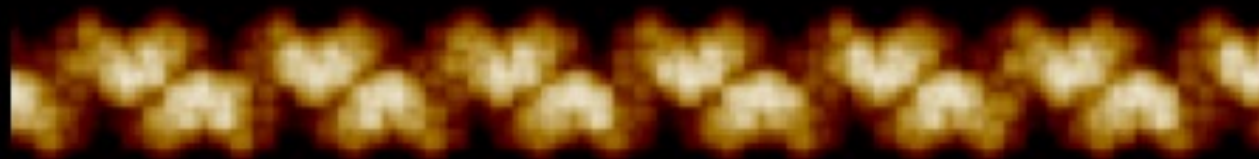
3.0 nm
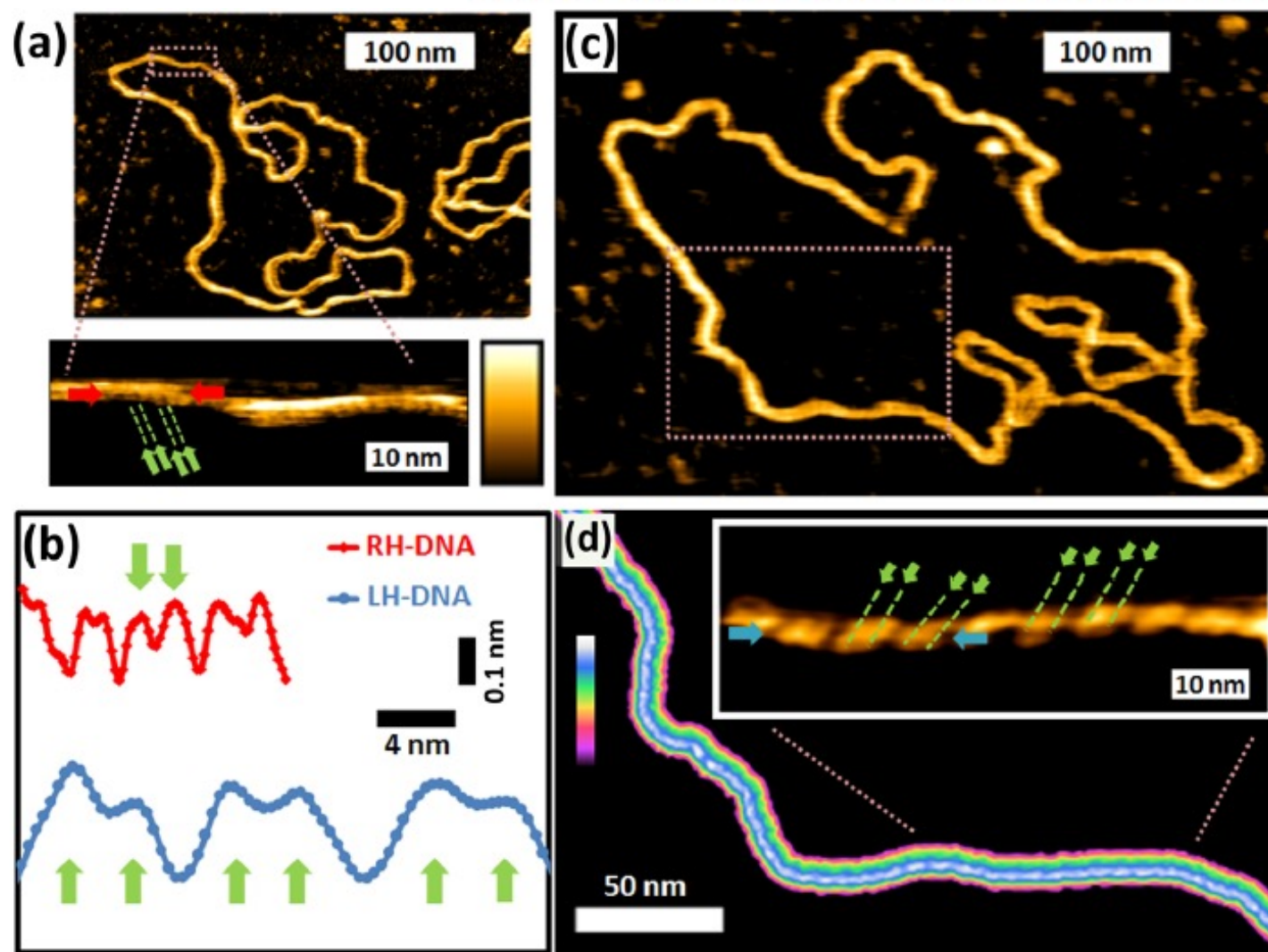
Figure 4. High-resolution AFM on plasmid DNA. (a) 3486 bp plasmid DNA, which on magnification shows a right-handed double helix, superposed to substantial height differences on and along the DNA. (b) Profiles along right-handed (RH) and left-handed (LH) DNA, acquired along the lines marked by the red and blue arrows in the insets of A and D. (c) Elongated configuration of the 3486 bp plasmid DNA displayed at the same scale as part a. (d) On subsequent magnifications of the dashed rectangle in c, an elongated left-handed double helix is resolved. Color scale: 1.5 nm (a); 1.1 nm (a, inset); 1.5 nm (c); 1.1 nm (d); 0.7 nm (d, inset). Green arrows indicate the two strands of the double helix, separated by the minor groove (depth ≲0.1 nm). The major groove (depth ∼0.2 nm) separates the subsequent turns of the double helix.

DNA adhesion on mica

DNA negatively charged

Divalent Cations (e.g., Ni++, Mg++)

Polycations (spermidine, polyornithine)

Mica

Courtesy of C. Rivetti

MICA

Biotite

tetrahedral layer

octahedral layer

M2 M1

K

O

Si

O (OH)

Al

O (OH)

Si

O

4.64 A

(001)

(a)

b

c

Si^{4+}

Al^{3+}

K$^+$

O^{2-}

OH$^-$

(b)

b
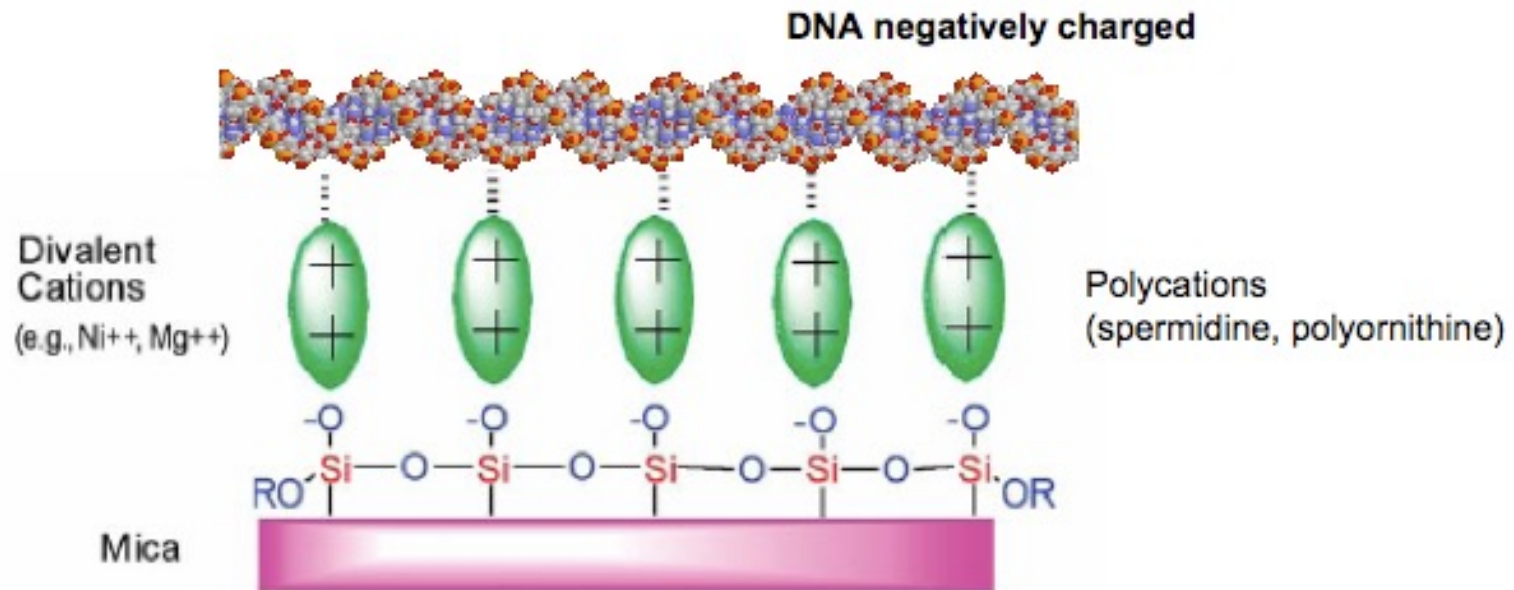
a
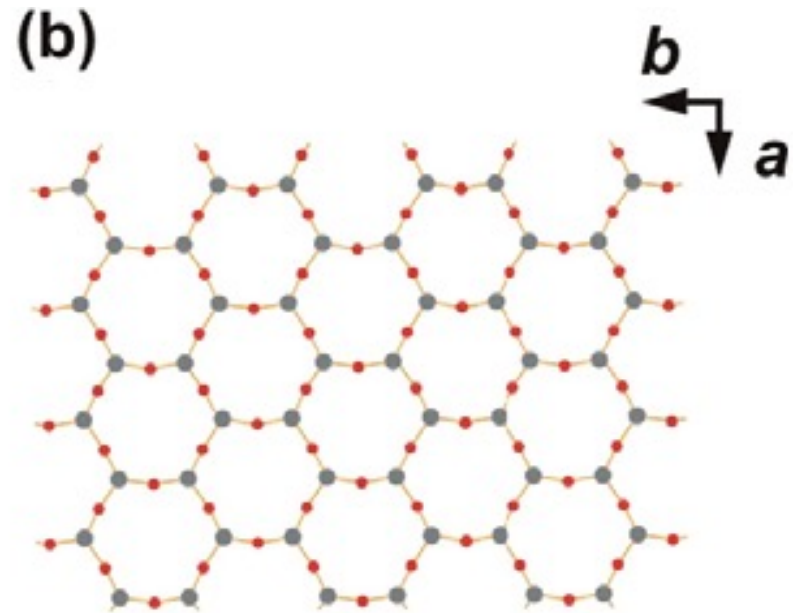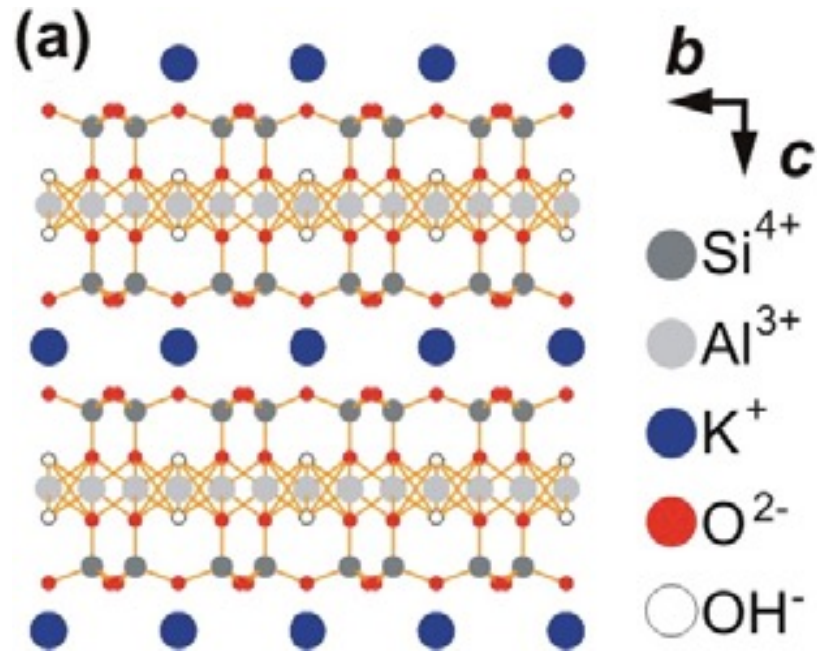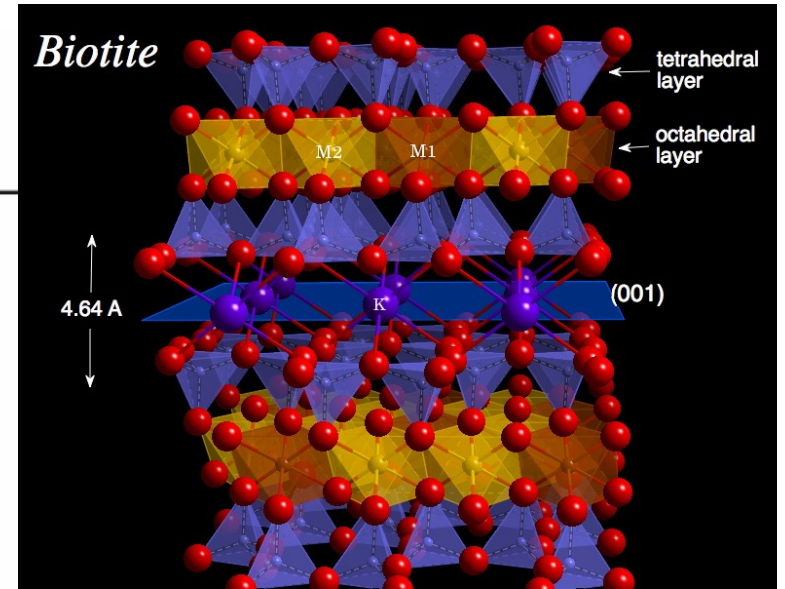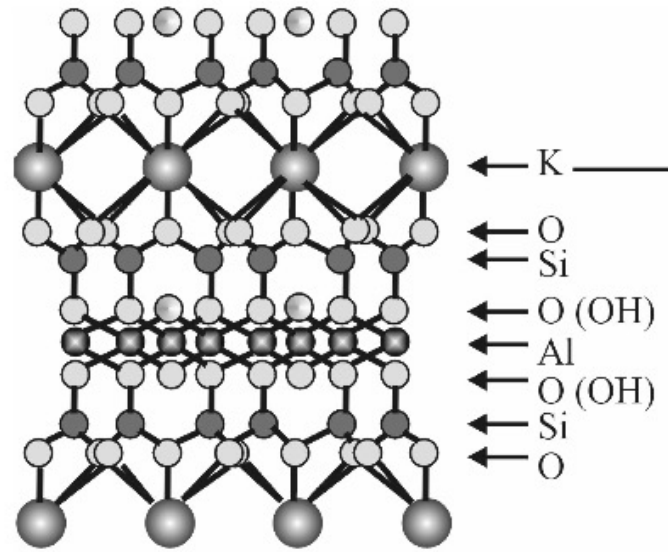
DNA deposition methods
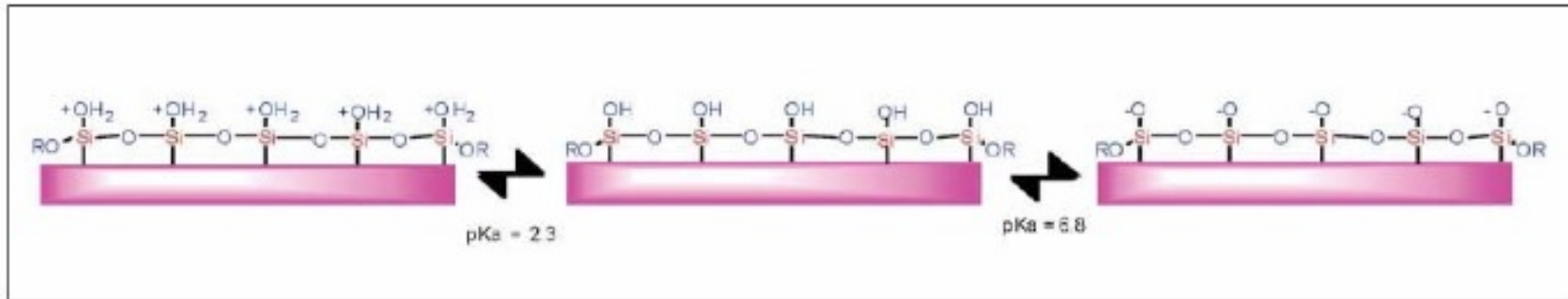
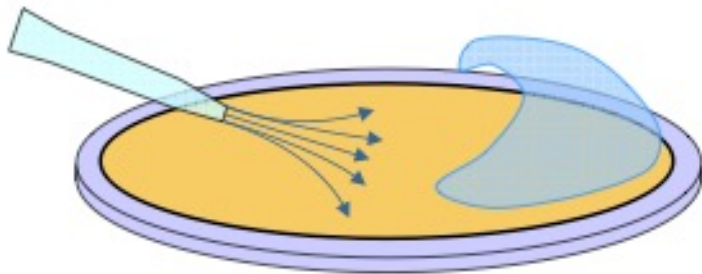Figure 1. Siloxy groups on the surface of freshly cleaved mica.
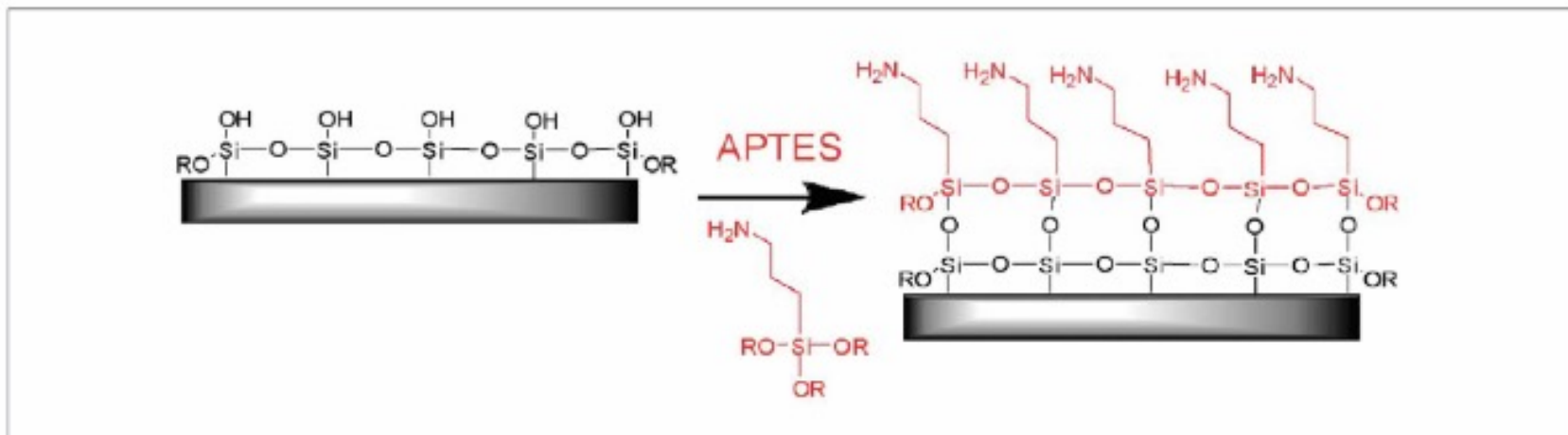
Figure 2. APTES treated mica substrate.

Courtesy of C. Rivetti
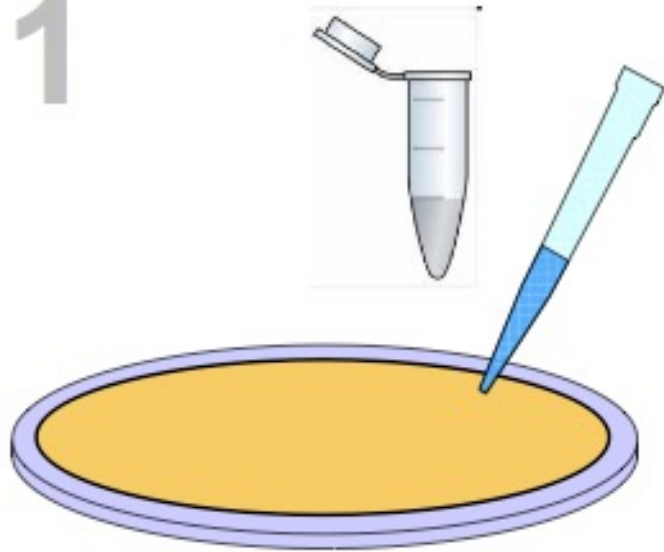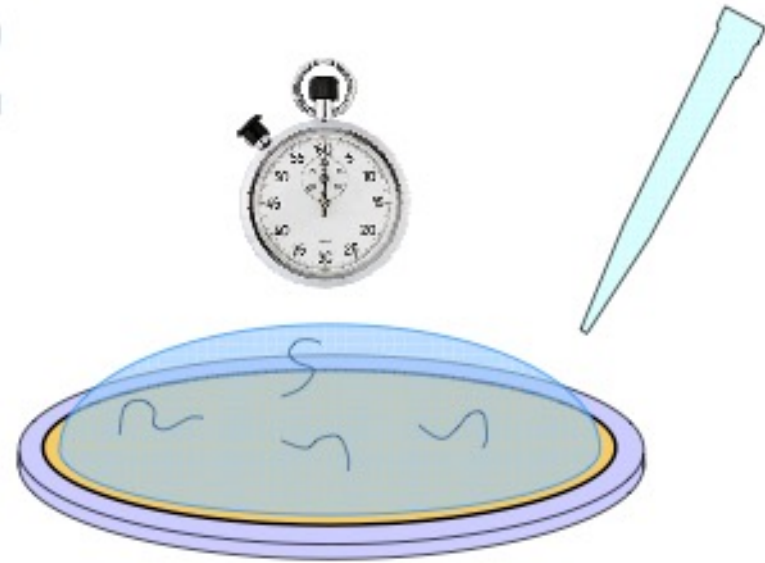
DNA deposition steps

N₂
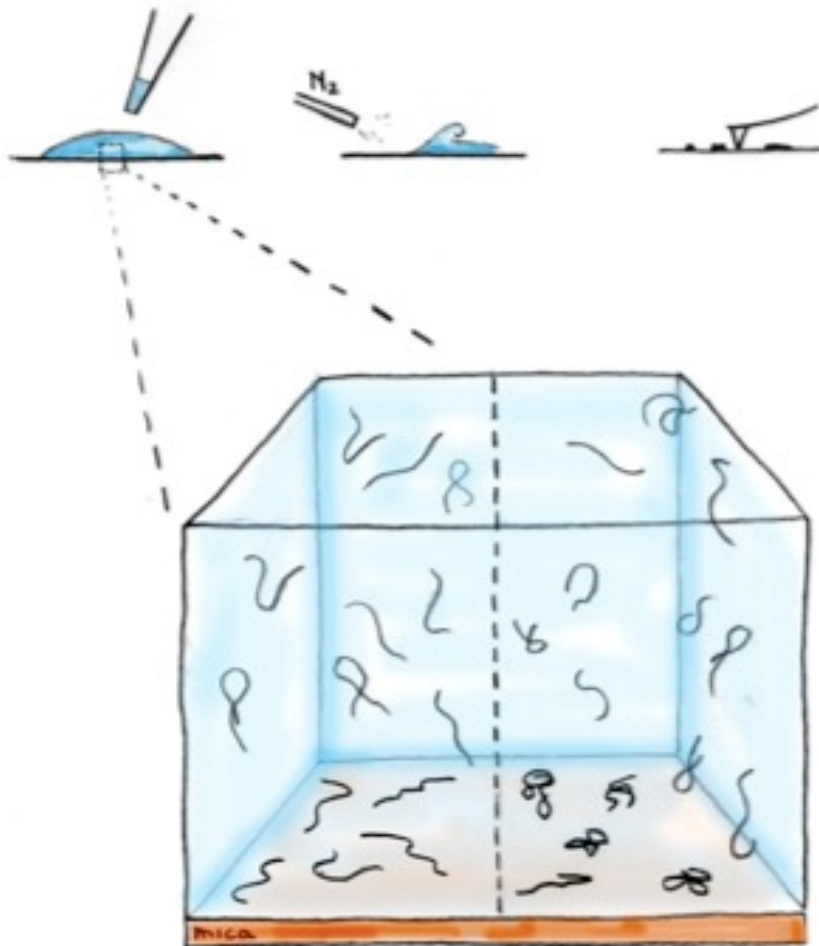
How do DNA molecules go from solution to the surface?

Once bound to the surface can they go back into solution?

What happens to the molecules on the surface before removing the buffer?
Can they move in 2D or are they trapped in a single conformation?

Can we quantitatively distinguish between the different cases?

mica

Courtesy of Prof. C. Bustamante

DNA Deposition onto Untreated and Treated Mica

Freshly cleaved — 2 μm

Glow discharged — 2 μm

H⁺-exchanged — 2 μm

4 nm / 0 nm

Courtesy of Prof. C. Bustamante
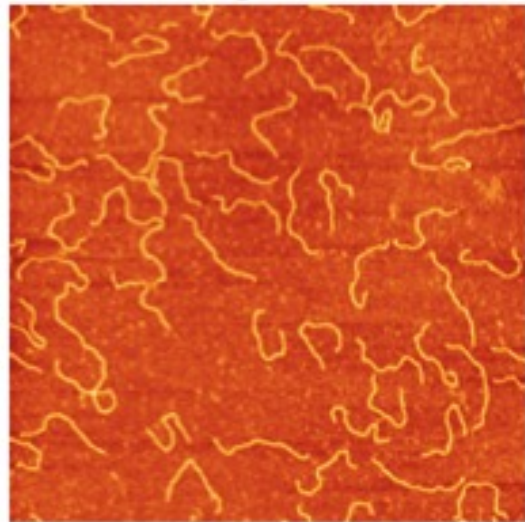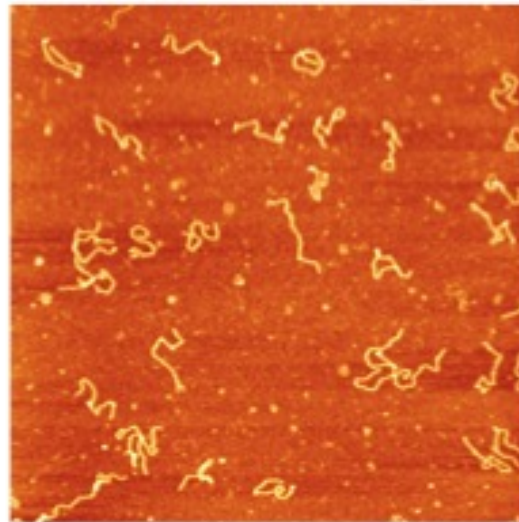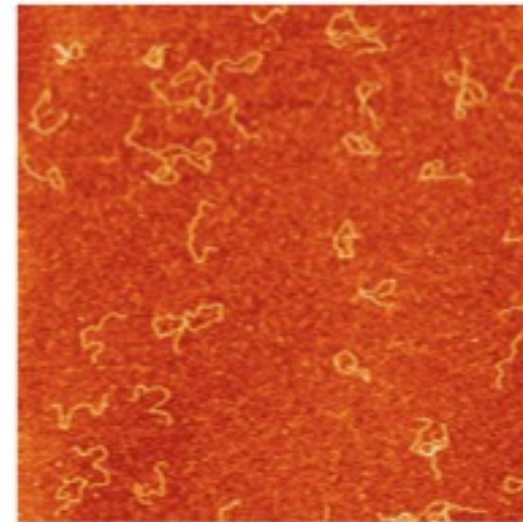
Number of DNA Molecules on the Surface vs. Time

On cleaved mica, transfer of DNA from solution to the surface is solely governed by diffusion:

$$n_F = \frac{\text{N. of Molecules}}{\text{Area}} = \frac{2}{\sqrt{\pi}} n_0 \sqrt{Dt}$$

n_0 initial DNA concentration in molecules/cm^3
D diffusion coefficient
t time of deposition
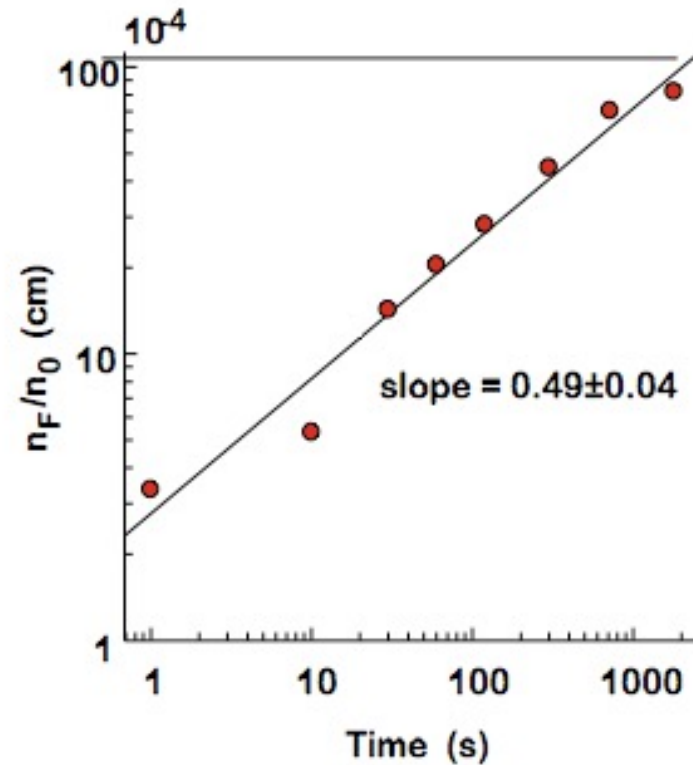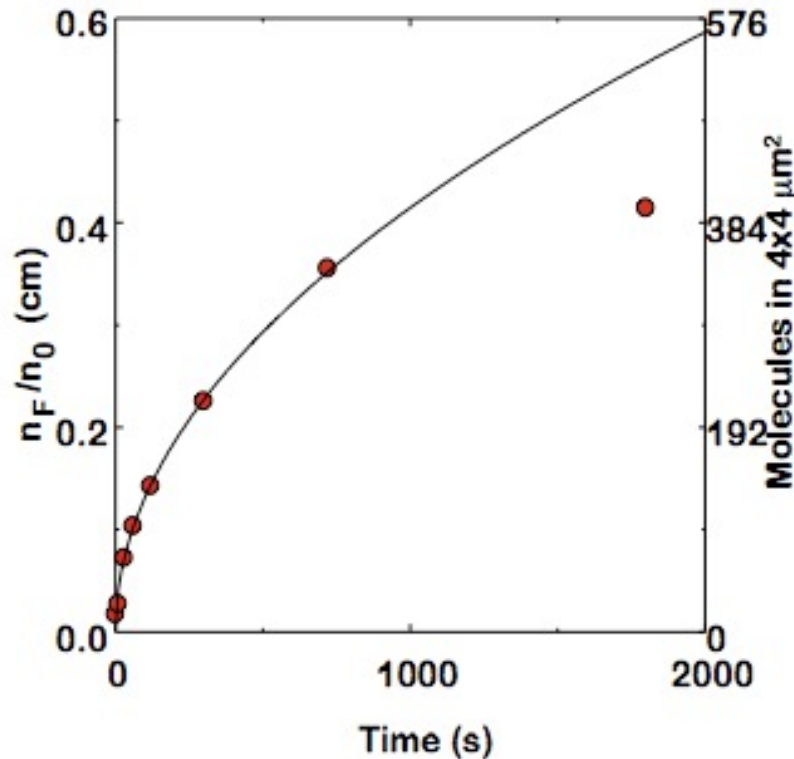
$$D = (5.4 \pm 0.2)10^{-8} \text{ cm}^2/\text{s}$$

Valid if:
- The molecules are irreversibly adsorbed to the surface
- Convection currents do not contribute to the transport of the molecules to the surface
- The solution is not significantly depleted of DNA molecules and the surface is not saturated during the time of deposition

Courtesy of Prof. C. Bustamante

Equilibrium Statistic of a Worm-like Chain

Isotropic rod continuously flexible. The worm-like chain model is particularly suited for describing stiffer polymers, with successive segments displaying a sort of cooperativity: all pointing in roughly the same u_1 direction
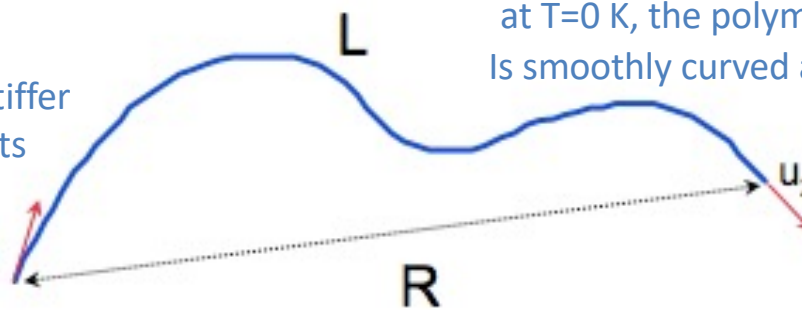
at T=0 K, the polymer adopts a rigid rod conformation Is smoothly curved at RT

$$\left\langle \vec{u_1} \cdot \vec{u_2} \right\rangle = e^{-\frac{L}{P}}$$

The persistence length of the molecule, P, is the decay length through which the initial orientation of the molecule persist. It is a measure of the stiffness of a polymer chain.

In 2D the mean square end-to-end distance of a worm-like chain of length L, and persistence length P, is:

$$\left\langle R^2 \right\rangle_{2D} = 4PL\left(1 - \frac{2P}{L}\left(1 - e^{-\frac{L}{2P}}\right)\right)$$

$$\text{For } L \rightarrow \infty \quad \left\langle R^2 \right\rangle_{2D} = 4PL$$

Courtesy of Prof. C. Bustamante

WLC is for semi-flexible polymers.
Assumes polymers are inextensible, has a linear elastic bending energy and is subjected to thermal fluctuations.
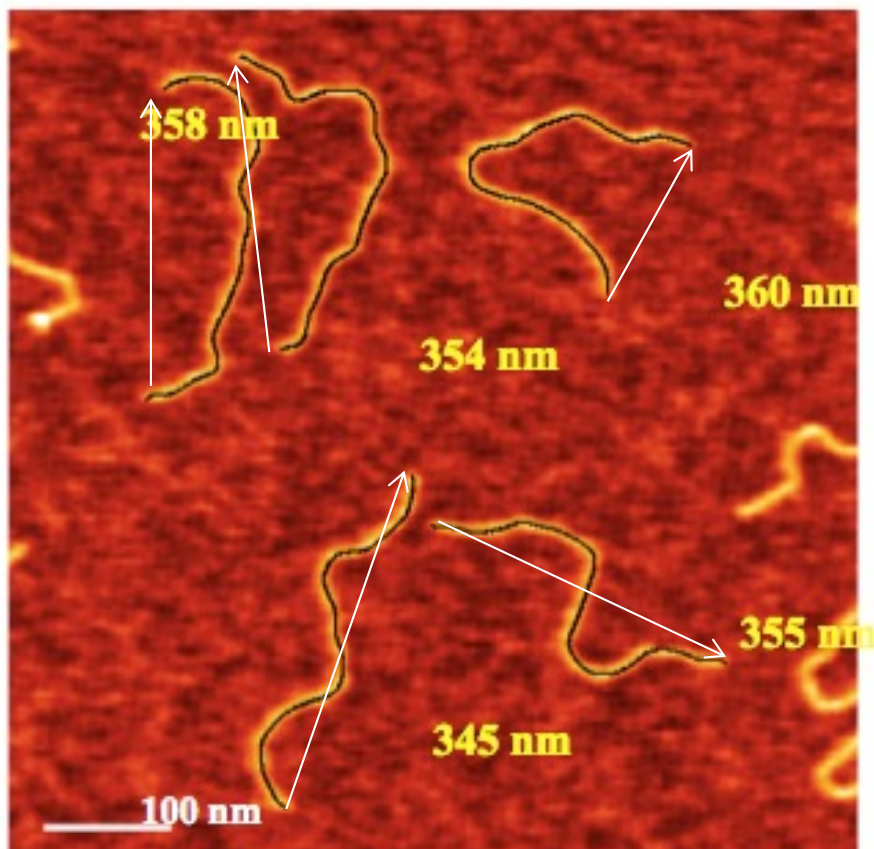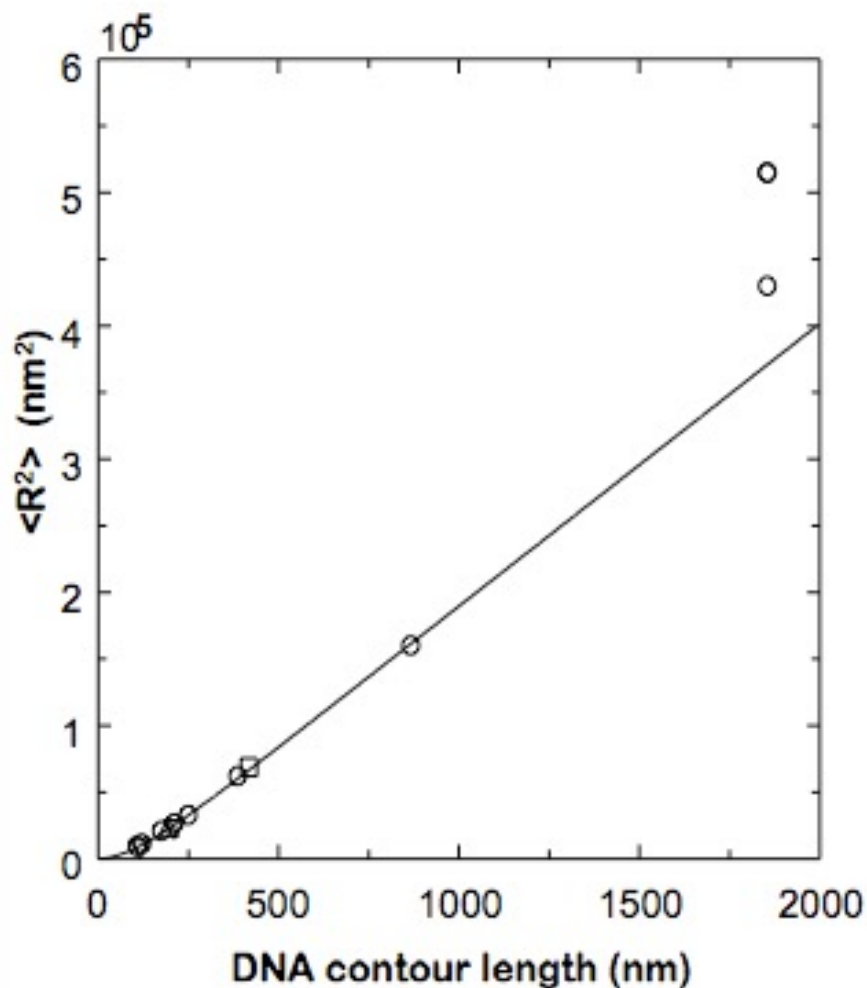
a) L=Nl segments, freely rotating
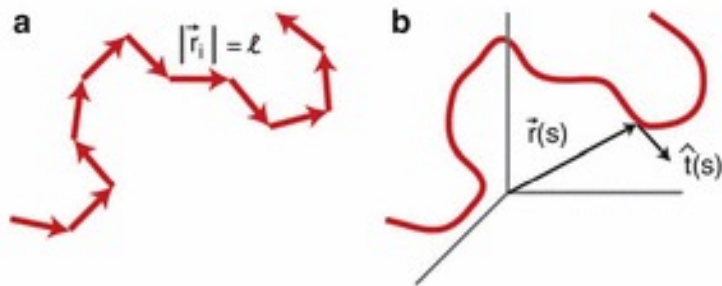
Worm-Like Chain (WLC) Model, Fig. 1 (a) Discrete model of a polymer composed of a chain of segments $\vec{r}_i$ each of length ℓ. (b) Continuous WLC polymer parameterized by the tangent vector $\vec{t}(s) = \frac{\partial \vec{r}(s)}{\partial s}$ along the contour

Adding energy cost associated to the bending:

$$H = -\varepsilon \sum_{i=1}^{N-1} \vec{r}_{i+1} \cdot \vec{r}_i, \qquad (1)$$

which imposes an energy cost of $\varepsilon \ell^2$ times the cosine of the angle between neighboring segments. The right-hand side of (1) can be rewritten using the relation $\vec{r}_{i+1} \cdot \vec{r}_i = \frac{2\ell^2 - (\vec{r}_{i+1} - \vec{r}_i)^2}{2}$. Moving from a discrete model to a continuous model requires taking the limits $N \to \infty$ and $\ell \to 0$. Likewise:

$$\lim_{\ell \to 0} \left(\frac{\vec{r}_{i+1} - \vec{r}_i}{\ell} \right) = \frac{\partial \vec{t}(s)}{\partial s}, \qquad (2)$$

where $\vec{t}(s)$ is a tangent vector at location s along the contour of the polymer (see Fig. 1b). Finally, converting the sum to an integral yields:

$$\frac{H}{k_B T} = \frac{\xi}{2} \int_0^L \left(\frac{\partial \vec{t}(s)}{\partial s} \right)^2 ds, \qquad (3)$$

WLC is for semi-flexible polymers.
Assumes polymers are inextensible, has a linear elastic bending energy and is subjected to thermal fluctuations.
a) L=Nl segments, freely rotating
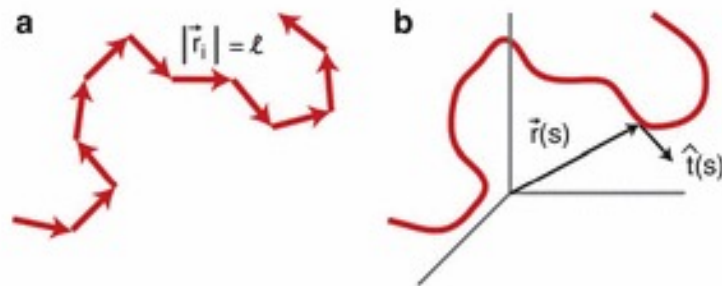
Worm-Like Chain (WLC) Model, Fig. 1 (a) Discrete model of a polymer composed of a chain of segments $\vec{r}_i$ each of length ℓ. (b) Continuous WLC polymer parameterized by the tangent vector $\vec{t}(s) = \frac{\partial \vec{r}(s)}{\partial s}$ along the contour

which is the Hamiltonian for the WLC model assuming that the contour length L is very large (Doi and Edwards 1988). Note the introduction of the persistence length $\xi = \frac{\epsilon \ell}{k_B T}$. The persistence length serves as a characteristic length scale over which two tangent vectors along the polymer remain correlated, i.e.:

$$\langle \vec{t}(s) \cdot \vec{t}(s') \rangle = e^{-\frac{|s-s'|}{\xi}}. \tag{4}$$

The WLC describes a polymer that is stiff over short distances and flexible at longer ones, with the persistence length setting the length scale of this transition in characteristic behavior. Moreover, while

Mean Square End-to-End Distance of DNA Molecules vs. their Contour Length

Courtesy of Prof. C. Bustamante and C. Rivetti

$$\langle R^2 \rangle_{3D} = 2PL\left(1 - \frac{P}{L}\left(1 - e^{-\frac{L}{P}}\right)\right)$$

$$\langle R^2 \rangle_{2D} = 4PL\left(1 - \frac{2P}{L}\left(1 - e^{-\frac{L}{2P}}\right)\right)$$

$$\langle R^2 \rangle_{proj} = \langle R_x^2 \rangle + \langle R_y^2 \rangle = \frac{2}{3}\langle R^2 \rangle_{3D}$$

Theoretical model for a 1258 bp DNA	$\langle R^2 \rangle$ nm^2
Ideal worm-like chain in 3D	35600
Ideal worm-like chain in 2D	60500
Orthogonal 3D → 2D projection	23700

$\langle R^2 \rangle = 61300$ nm^2 $\qquad$ $\langle R^2 \rangle = 26000$ nm^2 $\qquad$ $\langle R^2 \rangle = 25100$ nm^2
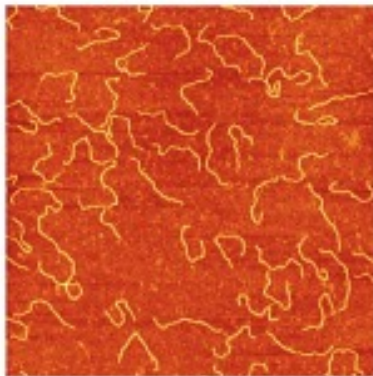
Freshly cleaved $\qquad$ Glow discharged $\qquad$ H$^+$-exchanged
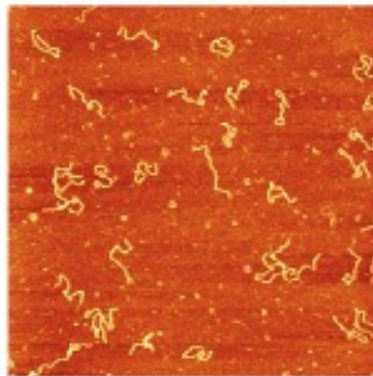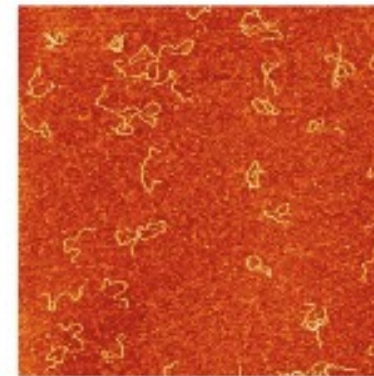
Courtesy of Prof. C. Rivetti

AFM under Liquid
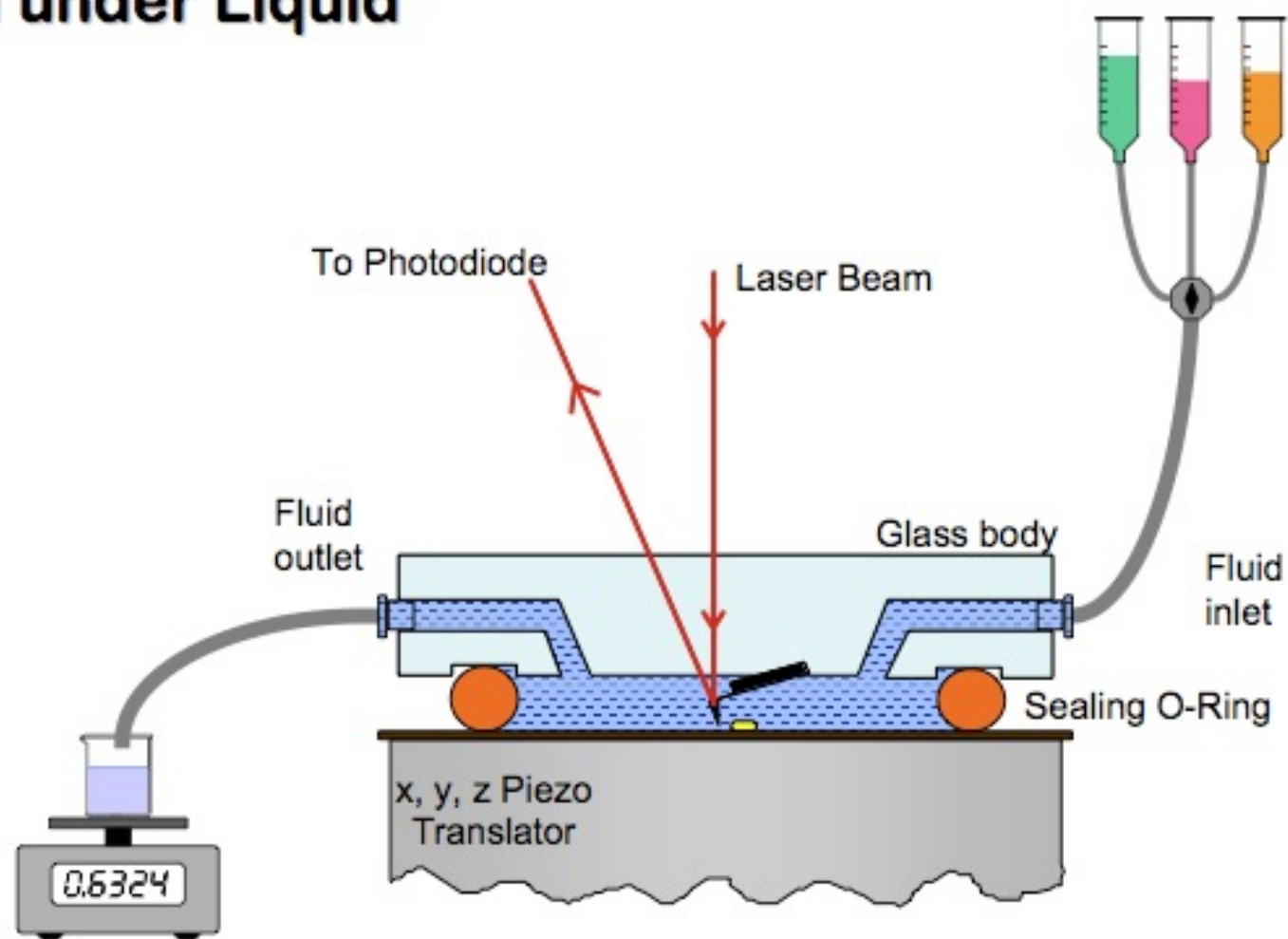
Courtesy of Prof. C. Rivetti

DNA imaged in liquid
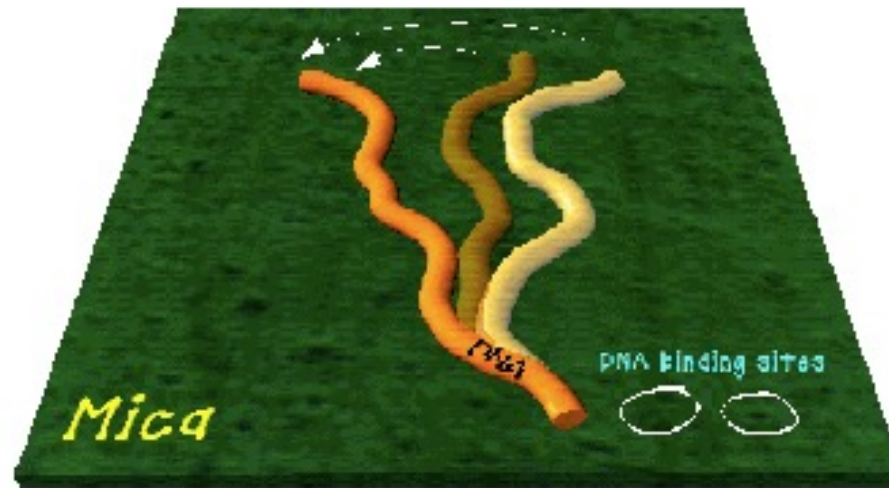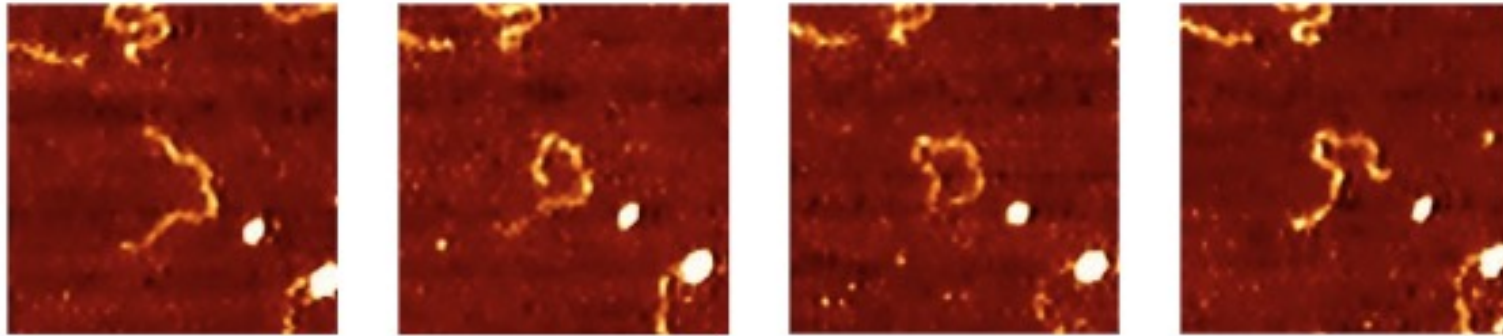
Courtesy of Prof. C. Rivetti

DNA bend angle measurements

A-tract

10 bp

| AAAAACGCG | AAAAACGCG | AAAAACGCG | AAAAACGCG |
| TTTTTGCGC | TTTTTGCGC | TTTTTGCGC | TTTTTGCGC |
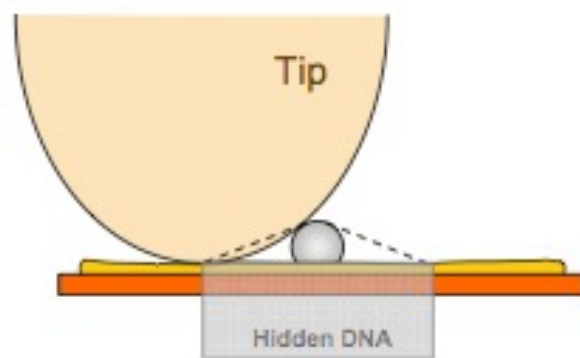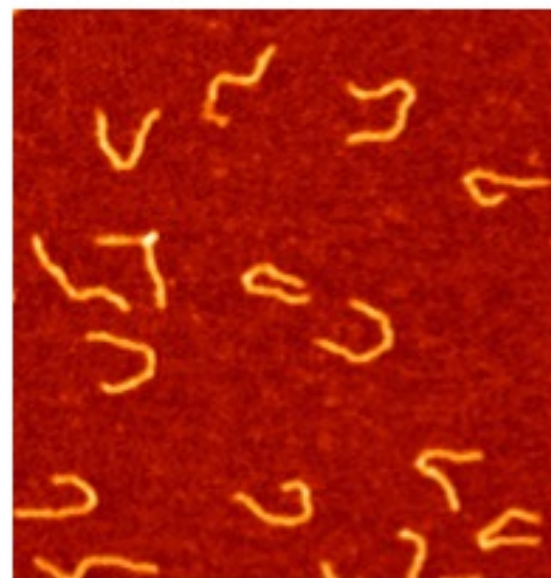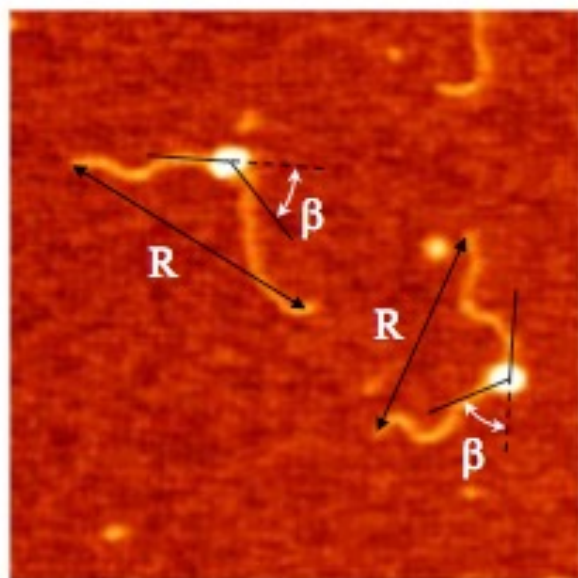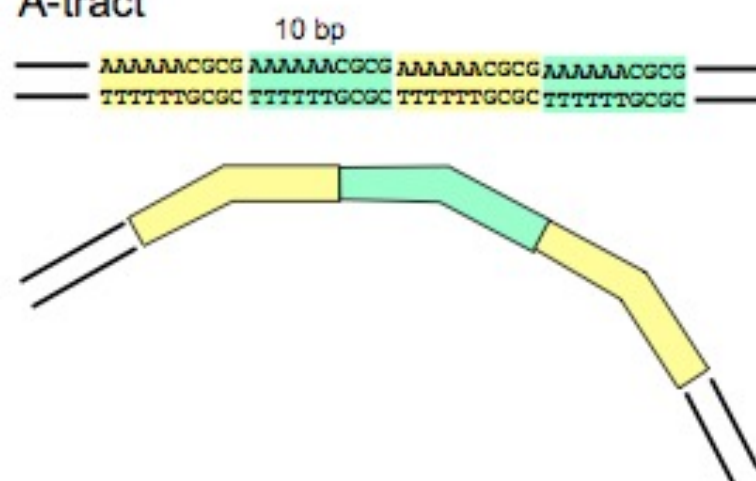
Using the end-to-end Distance to Determine Bend Angles

For a polymer molecule that is bent at any location along the chain, the mean square end-to-end distance is given by:
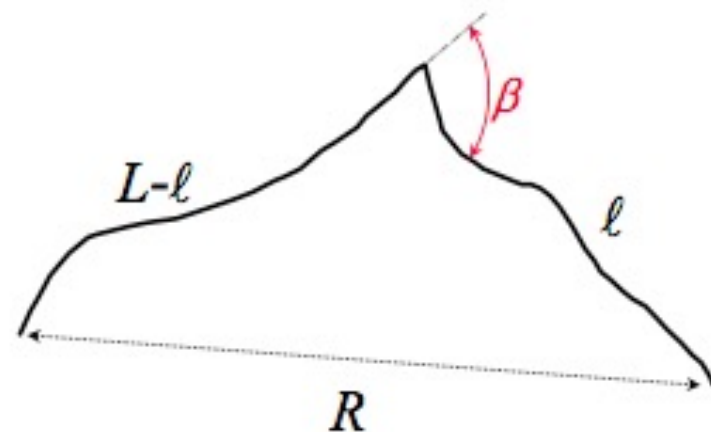
$$\left\langle R_\beta^2 \right\rangle_{2D} = 4PL\left\{1 - \frac{2P}{L}\left[\left(1 - e^{-\ell/2P}\right) + \left(1 - e^{-(L-\ell)/2P}\right) - \cos(\beta)\left(1 - e^{-\ell/2P}\right)\left(1 - e^{-(L-\ell)/2P}\right)\right]\right\}$$

DNA fragments containing A-tracts

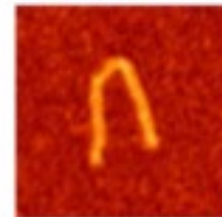2 A-tracts
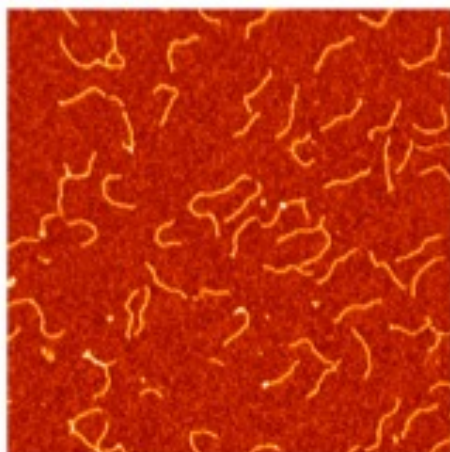
4 A-tracts
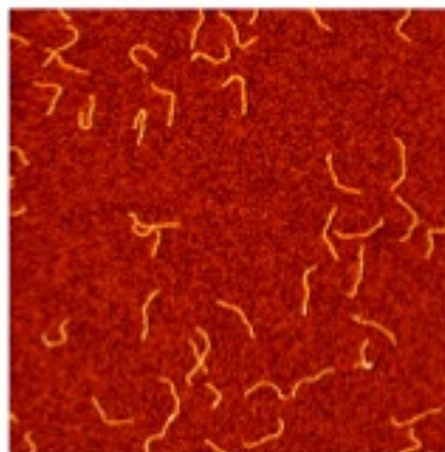
6 A-tracts
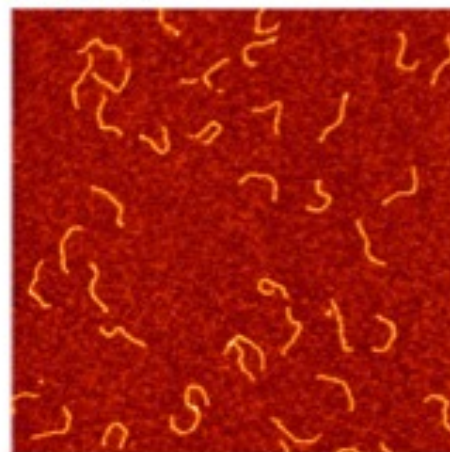
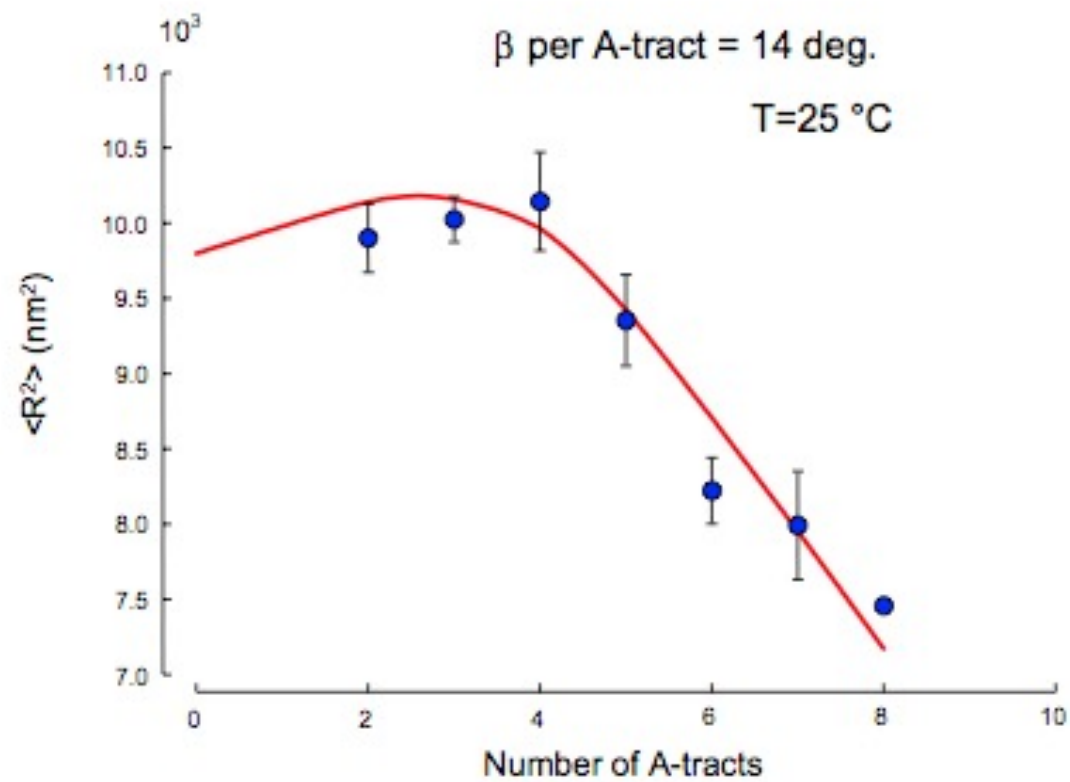8 A-tracts
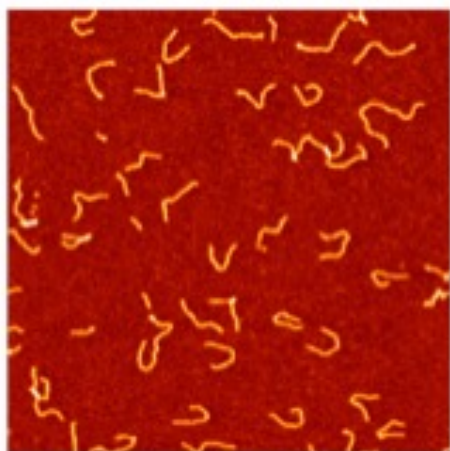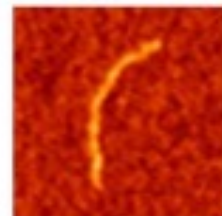
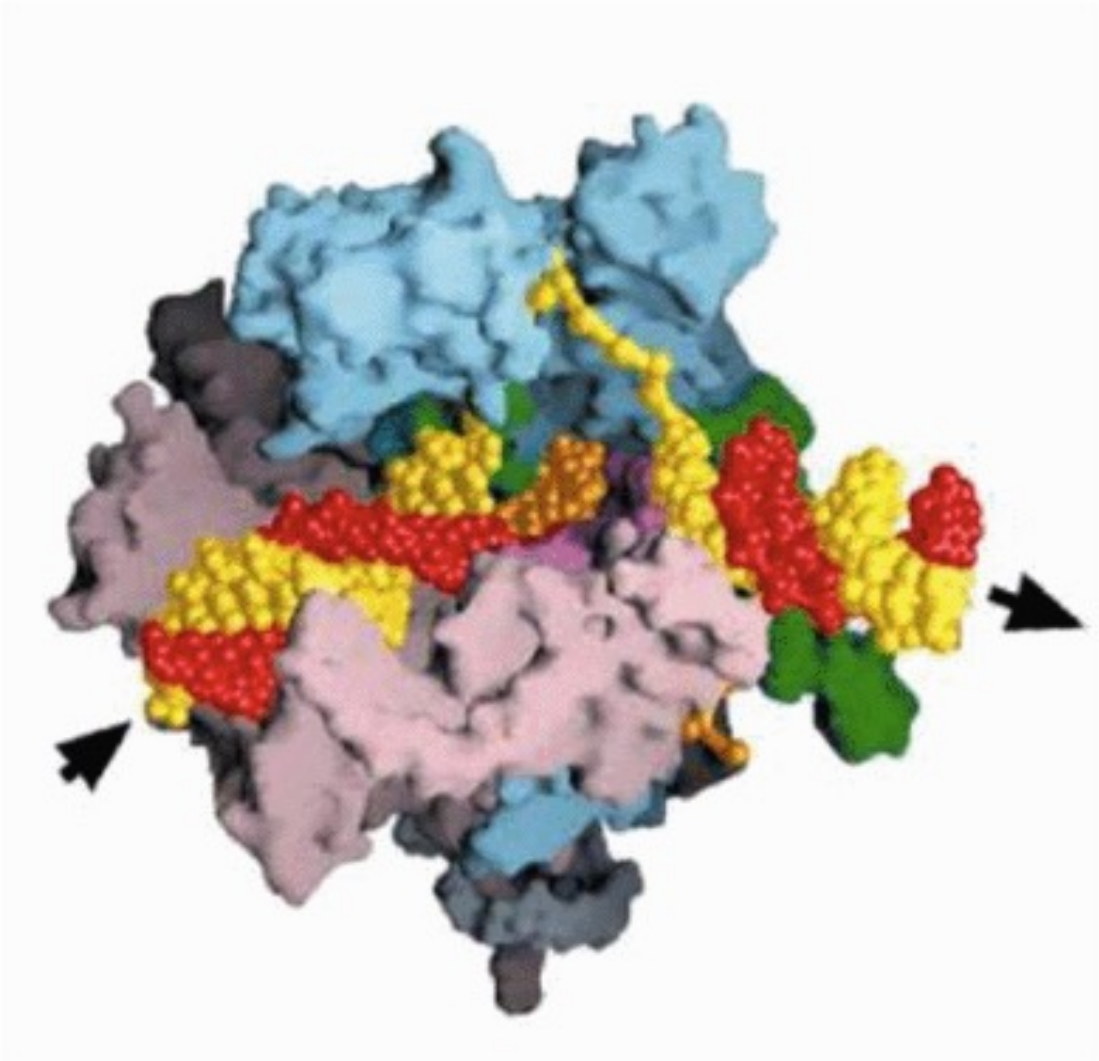2 A-tracts

3 A-tracts
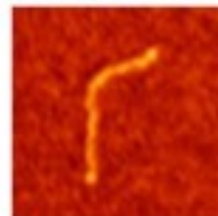
4 A-tracts
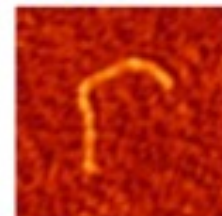
5 A-tracts
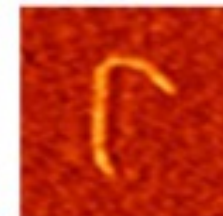
6 A-tracts
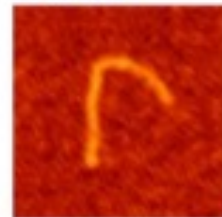
7 A-tracts

8 A-tracts

2 μm
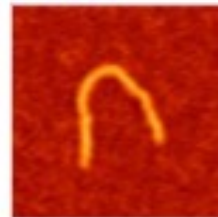
50 nm

Mean square end-to-end distance as a function of the number of A-tracts

β per A-tract = 14 deg.

T=25 °C

155 bp   [AAAAAACGCG]$_{n=1-8}$ 206 bp

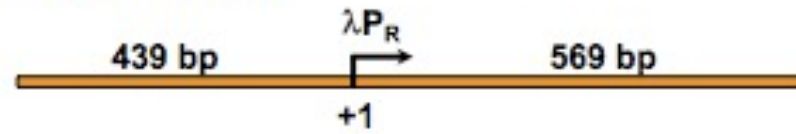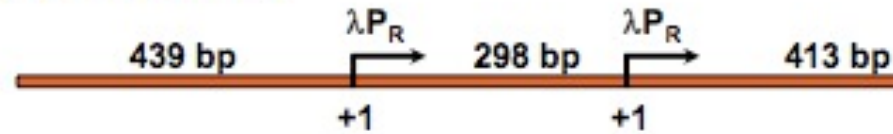# Structure of the E. coli RNA Polymerase

Courtesy of Prof. C. Rivetti

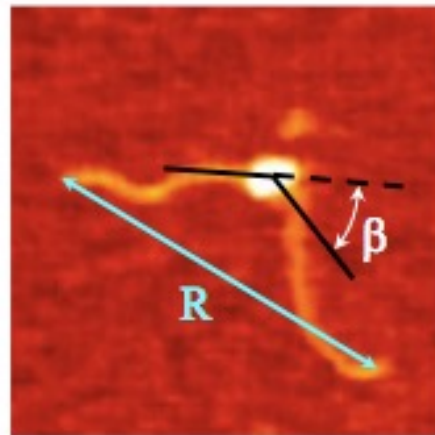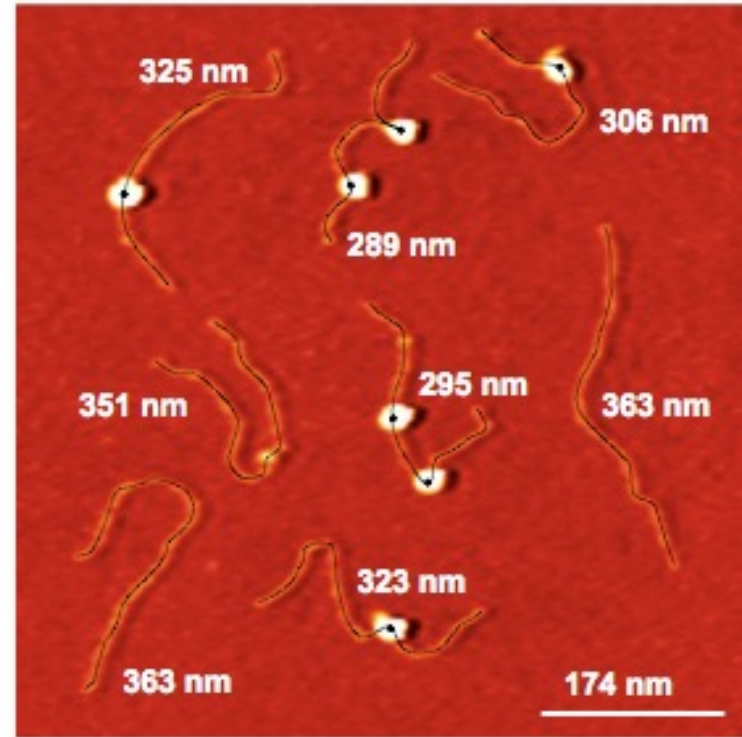Courtesy of Prof. C. Rivetti

AFM image of Open Promoter Complexes
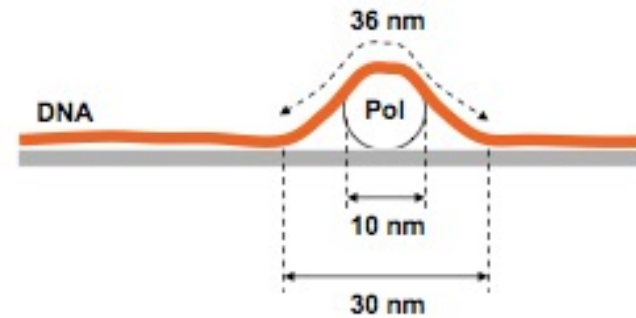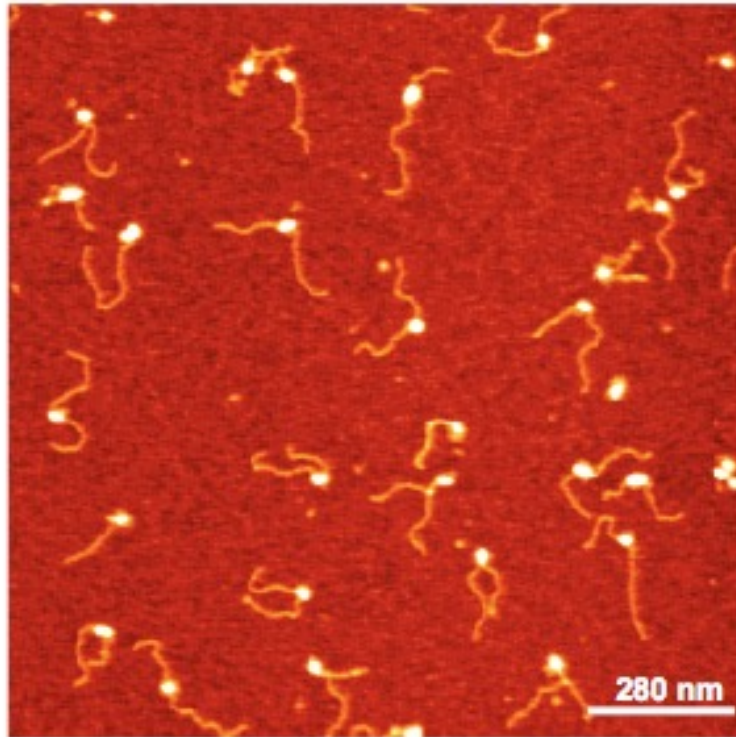
Courtesy of Prof. C. Rivetti

DNA Contour Length Measurements of Open Promoter Complexes

OPC on Template A

Legend:
- DNA (red)
- OPC (green)

Y-axis: Number of molecules (0, 30, 60, 90, 120)
X-axis: Contour Length (nm) (200, 250, 300, 350, 400)

OPC on Template C (2 λ_{PR})

Legend:
- DNA (red)
- 1 OPC (green)
- 2 OPC (yellow)

Y-axis: Number of molecules (0, 10, 20, 30, 40, 50, 60)
X-axis: Contour Length (nm) (240, 260, 280, 300, 320, 340, 360, 380, 400)
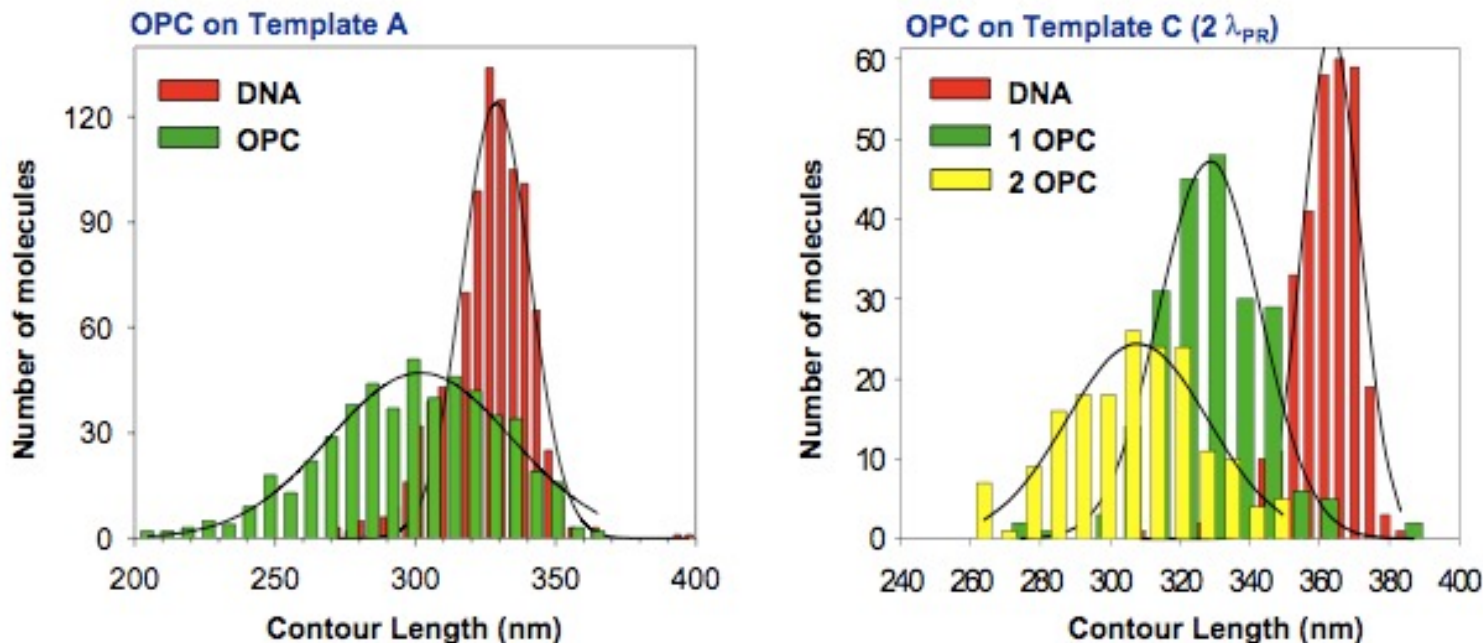
	Contour length (nm)	Compaction (nm)	N. of molecules
DNA (A)	329 ± 12		947
OPC (A)	297 ± 34	32	514
DNA (C)	363 ± 8		317
One OPC (C)	332 ±14	31	157
Two OPC (C)	308 ± 20	55	173

(a)

NO wrapping (side view)

NO wrapping (top view)

Wrapping (top view)

$L = 6.1d$

$\ell = 5.5d$

$L = 6.1d$ $\ell = 3.5d$
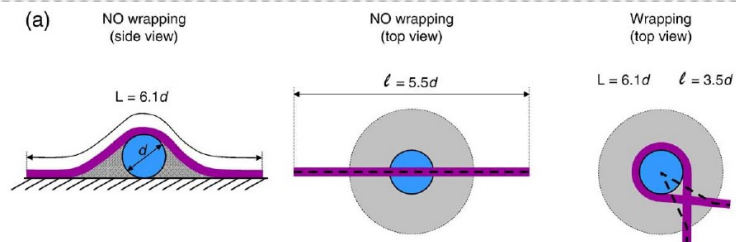
Proposed model for the open promoter complex at λ_{PR}

Courtesy of Prof. C. Rivetti